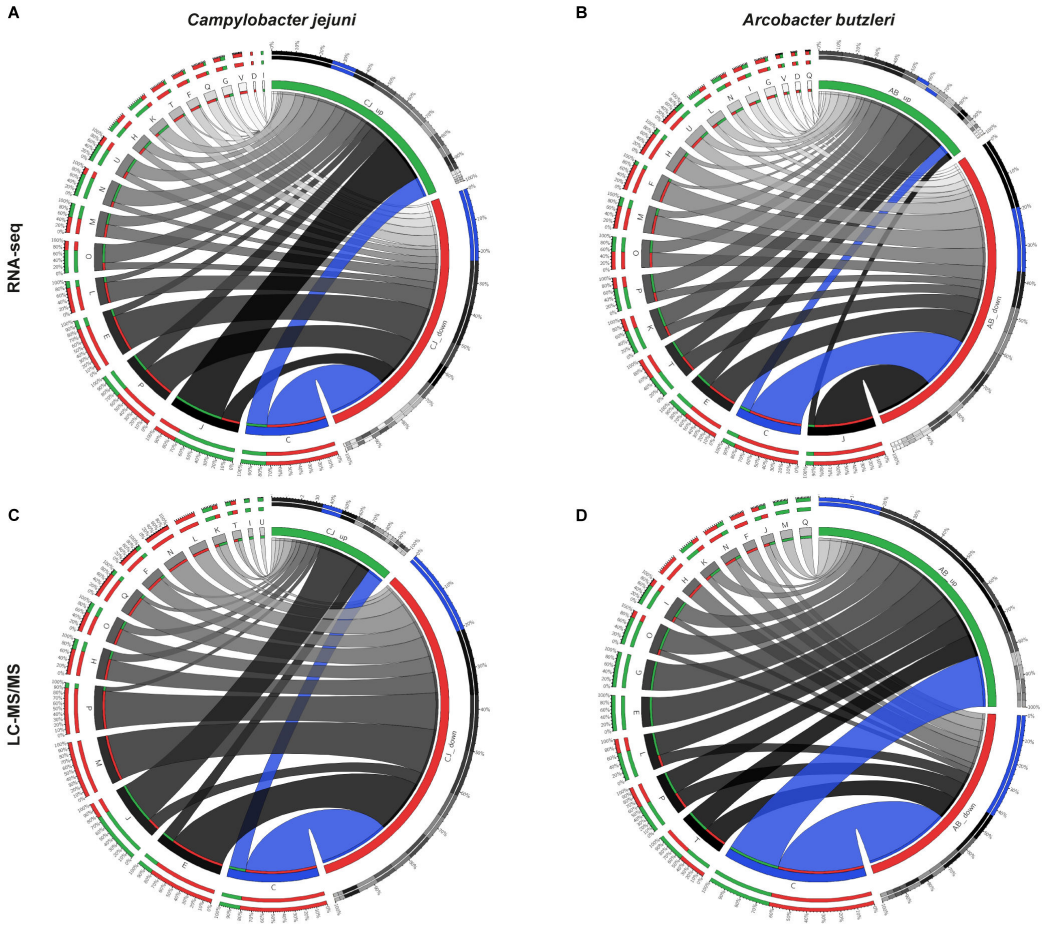

FIG 4 Impact of Cj1608 and Abu0127 on gene regulation in *C. jejuni* and *A. butzleri*, respectively. (A) Circos plots presenting the correlation between COG and differentially expressed *C. jejuni* genes revealed by RNA-seq in the ΔCj1608 strain compared to the *C. jejuni* wild-type strain. (B) Circos plots presenting the correlation between COG and differentially expressed *A. butzleri* genes revealed by RNA-seq in the ΔAbu0127 strain compared to the *A. butzleri* wild-type strain. (C) Circos plots presenting the correlation between COG and differentially expressed *C. jejuni* proteins revealed by LC-MS/MS in the ΔCj1608 strain compared to the *C. jejuni* wild-type strain. (D) Circos plots presenting the correlation between COG and differentially expressed *A. butzleri* proteins revealed by LC-MS/MS in the ΔAbu0127 strain compared to the *A. butzleri* wild-type strain. (A–D) Expression changes of $|\log_2 FC| \geq 1$ and FDR < 0.05 were considered significant and were included in the analyses. The category of unknown genes was excluded from the analysis. COG, Cluster of Orthologous Groups.

production under various O_2 supplies. Under 1% O_2, the ΔCj1608 strain grew faster than WT and C_{Cj1608} strains, suggesting that the metabolic state of the ΔCj1608 mutant strain was optimized for reduced O_2 concentration (Fig. 5G). Under optimal O_2 level, CJ and C_{Cj1608} strains grew faster than under 1% O_2 and faster than the ΔCj1608 strain under 5% O_2, indicating that metabolic pathways of CJ and C_{Cj1608} strains were adjusted to increased O_2 availability, while the metabolism of ΔCj1608 was not. Under increased O_2 concentration, all three strains grew slower than under optimal conditions, with the ΔCj1608 strain growing slower than the CJ and C_{Cj1608} strains. The ATP analyses indicated that the relative ATP levels corresponded to the bacterial growth rates. The ATP level of the CJ strain under optimal microaerobic growth was assumed to be 100%. Compared to that, the level of ATP in the CJ strain under reduced O_2 concentration dropped to 38% ± 4%; at increased O_2 concentration, the level of ATP also decreased to 51% ± 7% (Fig. 5F; see Discussion). Under optimal conditions in the ΔCj1608 mutant

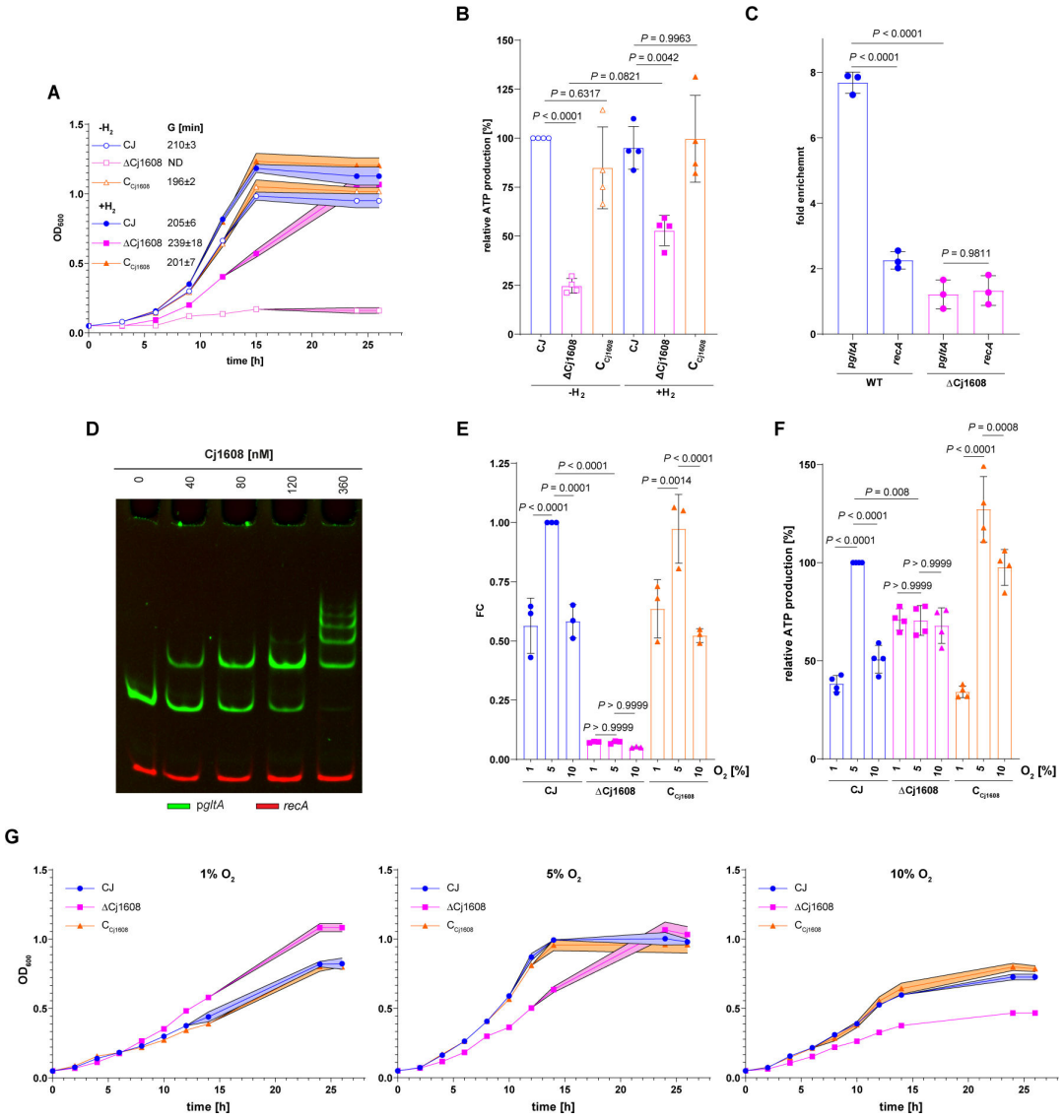

FIG 5 Cj1608-dependent control of *C. jejuni* energy conservation pathways. (A) Growth curves and generation times of CJ, ΔCj1608, and C_{Cj1608} strains cultivated in the presence of H_2 or without H_2. (B), ATP production by CJ, ΔCj1608, and C_{Cj1608} strains cultivated as in part A. (C) ChIP-qPCR analysis of p*gltA* fragment immunoprecipitated from CJ and ΔCj1608 cultured under microaerobic conditions; the *recA* gene was used as a negative control which Cj1608 does not bind. (D) EMSA analysis of Cj1608 binding to the p*gltA*-FAM promoter region *in vitro*; the *recA*-Cy5 fragment was used as a negative control. (E) RT-qPCR analysis of *gltA* transcription in CJ, ΔCj1608, and C_{Cj1608} cells cultured at different oxygen concentrations: (i) 1% O_2, (ii) 5% O_2, or (iii) 10% O_2 (see Materials and Methods). (F) Growth curves of CJ, ΔCj1608, and C_{Cj1608} strains cultivated as in panel E. (G) ATP production by CJ, ΔCj1608, and C_{Cj1608} strains cultivated as in panel E. (A–C and E–G) Data presented as the mean values ± SD. Ordinary one-way ANOVA with Tukey's multiple comparison test determined the *P* value. *n* = 3 biologically independent experiments. ANOVA, analysis of variance; ChIP-qPCR, chromatine immunoprecipitation quantitive PCR; CJ, *C. jejuni* wild type; C_{Cj1608}, Cj1608 complementation mutant; ΔCj1608, Cj1608 knock-out mutant ; EMSA, Electrophoretic mobility shift assay; G, generation time; ND, non-determined; RT-qPCR, Reverse transcription quantitative PCR.

strain, the ATP level reached approximately 70% ± 8% of that in the CJ strain and was constant regardless of increased or decreased O_2 supply. The ATP levels in the C_{Cj1608} strain analyzed at different O_2 levels resembled that of the CJ strain. Thus, the results indicated that the ΔCj1608 mutant strain could not adjust pathways responsible for energy conservation to changing O_2 levels.

To summarize *C. jejuni*'s results, Cj1608 helps *C. jejuni* control pathways that are important for energy conservation and are dependent on oxygen availability. As we have

shown using the *gltA* gene as an example, Cj1608 directly controls gene expression in response to changing O_2 concentrations and oxidative stress.

Abu0127 controls *nuo* expression, ATP level, and growth in response to O_2 supply

Next, we examined the impact of Abu0127 on *A. butzleri's* growth. As for *C. jejuni*, the presence or absence of H_2 did not significantly affect the growth of the wild-type AB strain nor ATP level in AB cells under microaerobic conditions (Fig. 6A). In the presence of H_2, the ΔAbu0127 strain grew slower than the AB strain (Fig. 6A), and the ATP level of ΔAbu0127 cells reached 77% ± 3% of that in the WT cells (Fig. 6B). However, the ΔAbu0127 culture entered the stationary phase at OD_{600} comparable to that of the AB strain. Under microaerobic conditions without H_2, the growth and ATP level of ΔAbu0127 was further lowered; ΔAbu0127 ATP level reached 57% ± 3% of the AB cells, and cells entered stationary phase at lower OD_{600} than the wild-type AB strain (Fig. 6A and B). Despite many attempts, we could not construct an Abu0127 complementation mutant, possibly due to the imperfect molecular biology tools dedicated to *A. butzleri* (10). Nonetheless, the results indicated that the ΔAbu0127 strain produced less energy than AB cells, and using H_2, the ΔAbu0127 cells could produce more energy and multiply more efficiently (38). This suggests a similar pattern of bypass of TCA-dependent energy production via oxygen-dependent oxidative phosphorylation to that observed in *C. jejuni*.

Next, we analyzed whether Abu0127 directly affects the Nuo complex activity. We studied the expression of *nuoB* since it is the second gene of the *nuoA-N* operon, whose expression was severely downregulated in the ΔAbu0127 strain at the transcription and translation levels (Fig. S9A and B; S3 Data). We confirmed the interaction of the Abu0127 protein with the *nuoA-N* promoter region *in vivo* by ChIP-qPCR and *in vitro* by EMSA (Fig. 6C and D), and we found that it was specific because Abu0127 did not interact with control *A. butzleri gyrA* and *recJ* regions, respectively. Next, we used RT-qPCR to analyze *nuoB* transcription under paraquat-induced oxidative stress and different O_2 supply. It should be noted that *A. butzleri* can grow under aerobic conditions (40); thus, aerobic O_2 concentration is less harmful to *A. butzleri* than to *C. jejuni*. The transcription of *nuoB* changed across different O_2 concentrations, being the lowest at 1% O_2 (FC of 0.61 ± 0.06 compared to AB under 5% O_2) and highest at 10% O_2 (FC of 1.7 ± 0.27 compared to AB under 5% O_2) (Fig. 6E). Under optimal O_2 conditions, *nuoB* transcription was lower in the ΔAbu0127 strain than in the AB strain (FC of 0.3 ± 0.05 compared to AB under 5% O_2), and it was invariant across different O_2 concentrations (Fig. 6H). Paraquat-induced oxidative stress affected *nuoB* transcription neither in the wild-type AB nor ΔAbu0127 strain, confirming the transcriptomic results (Fig. S9C, S3 Data). Next, we analyzed *A. butzleri* growth and ATP production under various O_2 supplies. Under 1% O_2, the AB and ΔAbu0127 strains grew similarly. However, ΔAbu0127 reached a lower OD_{600} at the stationary growth phase than the AB strain (Fig. 6F). Under optimal and increased O_2 concentrations, the AB strain grew similarly at both concentrations, faster than under 1% O_2, but reached a similar OD_{600} upon entry to a stationary growth phase as under 1% O_2. The ΔAbu0127 strain grew similarly under 5% and 10% O_2 but faster than under 1% O_2. Nonetheless, ΔAbu0127 grew slower than AB under the same conditions, and the culture finally reached a lower OD_{600} than AB (Fig. 6F). The relative ATP energy levels corresponded to the bacterial growth rates. The ATP level of the AB strain under microaerobic growth was assumed to be 100%. Compared to that, under 1% O_2, the level of ATP in the AB strain dropped to 44% ± 4%, while the level of ATP did not change in the culture grown at 10% O_2 (Fig. 6G). Under reduced O_2 concentration, the level of ATP in ΔAbu0127 was similar to that of the AB strain under the same conditions (35% ± 4% compared to AB under microaerobic growth). However, under 5% O_2, the ATP level of the ΔAbu0127 mutant strain reached 76% ± 3% of that in the AB strain and did not increase under 10% O_2. Thus, the results indicated that the ΔAbu0127 mutant strain could not

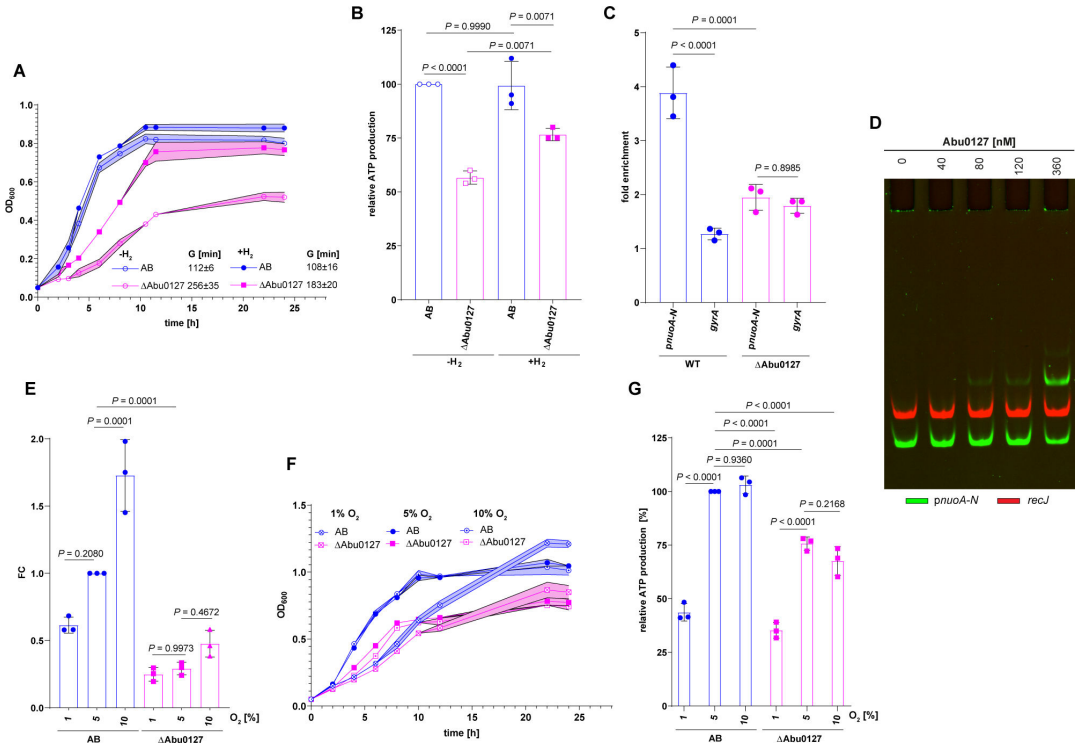

FIG 6 Abu0127-dependent control of *A. butzleri* energy conservation pathways. (A) Growth curves and generation times of AB and ΔAbu0127 strains cultivated in the presence of H_2 or without H_2. (B) ATP production by AB and ΔAbu0127 strains cultivated as in panel A. (C) ChIP-qPCR fold enrichment of DNA fragment in p*nuoA-N* by ChIP-qPCR in AB and ΔAbu0127 cultured under microaerobic conditions. The *gyrA* gene was used as a negative control not bound by Abu0127. (D) EMSA analysis of Abu0127 binding to the p*nuoA*-FAM promoter region *in vitro*; the *recJ*-Cy5 fragment was used as a negative control. (E) RT-qPCR analysis of *nuoB* transcription in AB and ΔAbu0127 strains cultured at different oxygen concentrations: (i) 1% O_2, (ii) 5% O_2, or (iii) 10% O_2 (see Materials and Methods). (F) Growth curves of AB and ΔAbu0127 strains cultivated as in panel E. (G) ATP production by AB and ΔAbu0127 strains cultivated as in panel E. (A–C, E–G) Data presented as the mean values ± SD. Ordinary one-way ANOVA with Tukey's multiple comparison test determined the *P* value. *n* = 3 biologically independent experiments. AB, *A. butzleri* wild type; ANOVA, analysis of variance; ΔAbu0127, Abu0127 knock-out mutant; ChIP, chromatin immunoprecipitation quantitative PCR; EMSA, electrophoretic mobility shift assay; G, generation time; RT-qPCR, reverse transcription quantitative PCR.

efficiently adjust pathways responsible for energy conservation to changing O_2 levels, in which it resembled *C. jejuni* ΔCj1608.

To summarize *A. butzleri*'s results, Abu0127 helps *A. butzleri* control pathways important for energy conservation dependent on oxygen availability. As we have shown using the *nuoB* gene as an example, Abu0127 directly controls gene expression in response to changing O_2 concentrations.

DISCUSSION

One of the challenges for a bacterial cell is to gain energy to grow and reproduce under different environmental conditions. Available energy sources and electron acceptors used for energy conversion are the two major factors defining the activity of metabolic pathways. The regulatory proteins redirect metabolism and ETC pathways, prioritizing electron donor or acceptor usage to maximize the energy gain (e.g., aerobic/microaerophilic over anaerobic respiration and fermentation or nitrate respiration over fumarate respiration). The fine-tuning of metabolism and respiration to particular conditions is usually hierarchical and orchestrated by multiple factors (41, 42), which often control the same genes. For example, in the model, facultative anaerobe *Escherichia coli*, but also other species of *Gammaproteobacteria*, three global transcriptional regulators, FNR, ArcA, and NarL/NarP, mainly control energy conservation processes dependent on the availability of electron acceptors (21, 43). In the energy reprogramming network, under low oxygen availability, FNR provides the first level of regulation, switching metabolism

from aerobic to anaerobic and controlling the expression of other transcriptional factors (44). ArcA, a response regulator of the ArcAB two-component system (45), possibly controls the switch between anaerobic respiration and fermentation, as well as the expression of a set of secondary regulators (46). NarL/NarP switches on nitrate and nitrite respiration when these electron acceptors are available while repressing genes for less effective anaerobic respiration (47). Studies have shown that the intensive cross-talk between regulatory proteins, often controlling the same genes hierarchically and controlling genes beyond energy conservation pathways, is essential for efficient bacterial responses or adaptation to diverse conditions (21, 48–50).

Until recently, no regulators redirecting energy conversion pathways in response to oxygen as an electron acceptor have been found in *Campylobacterota* (14, 51). It was experimentally shown that *C. jejuni* reprograms its metabolism upon changes to oxygen availability; nonetheless, the regulator remained unknown (39, 52). It was surprising, given that microaerobic species of this phylum must respond to changing oxygen levels, including harmful oxygen deficiency and excess.

In this and previous works (24, 26), we revealed that under microaerobic conditions, three homologous atypical response regulators, HP1021, Cj1608, and Abu0127, which we name *Campylobacteria* energy and metabolism regulators (CemR), control the expression of many genes involved in energy conversion, including TCA and ETC pathways [Fig. 3 and 4; Fig. S10; Supplementary Data 3 in reference (26)]. Indeed, when *cemR* genes were deleted, the most remarkable gene and protein expression changes occurred in energy production and conversion COG, reaching between 20% and 40% of all the downregulated genes or proteins (Fig. 4; Fig. S10; the category of unknown proteins was excluded from the study). Moreover, we showed that in strains lacking CemR, the transcriptional control was lost over the genes whose transcription was dependent on the oxygen level, e.g., *C. jejuni* TCA *gltA*, *A. butzleri* ETC, *nuoA-N* operon complex, *H. pylori*, TCA pyruvate:ferredoxin oxidoreductase *PFOR*, and ETC cytochrome c oxidase *ccoN-Q* [Fig. 5E and 6E and reference (26)]. Consequently, under microaerobic conditions in CemR deletion mutants of all three species, the ATP level and the growth rates were lower than in wild-type strains [Fig. 5F, G and 6F G, , and (26)]. The presence of CemR allowed *C. jejuni* and *A. butlzeri* to optimize energy conservation under microaerobic compared to reduced oxygen concentration, increasing the ATP level and bacterial growth rate (Fig. 5F, G and 6F G,). The lack of CemR specifically impaired pathways connected with oxygen utilization as an electron acceptor because in the presence of hydrogen as an alternative electron donor and proton motive force generator, *C. jejuni* and *A. butzleri* gained additional energy, allowing for faster growth (Fig. 5A, B and 6A B,). All these data indicate that CemR responds to oxygen levels and redirects metabolism toward optimal energy conservation. It is important to point out that data obtained from each single species would not have allowed us to conclude on the general role of CemR as an energy conservation regulator because, in each species, slightly different pathways were primarily controlled (e.g., TCA in *C. jejuni*, Nuo ETC in *A. butzleri*, and glucose uptake and pentose phosphate pathway in *H. pylori*). Nonetheless, the role of CemR in controlling other pathways or processes, often in a species-specific manner, still awaits detailed characterization.

An interesting question arises: how many energy conservation regulators are encoded in addition to CemR in each *Campylobacteria* species, and how do they all integrate into the regulatory circuits of a given species? *H. pylori*, *C. jejuni*, and *A. butzleri* differ in lifestyles, which shape the complexity of regulatory circuits, as recently illustrated using *Campylobacterota* as a representative phylum (20). *H. pylori* can be classified as a specialist bacterium (53), strictly human associated, using a limited repertoire of electron donors (hydrogen, pyruvate, 2-oxo-glutarate, malate, and succinate), and only oxygen or fumarate as electron acceptors during respiration (20). Oxygen, being a primary electron acceptor in *H. pylori*, is also toxic for *H. pylori* at higher than microaerobic concentrations (54). As a consequence of speciation and host adaptation, *H. pylori* lost many regulatory proteins. Nonetheless, the studies on

regulatory circuits in *H. pylori* indicated that HP1043 (55, 56), controlled by unknown stimuli, acid-responsive ArsRS (57), and metal-dependent regulators NikR and Fur (20, 58), affects *H. pylori* energy conversion to various extents in response to different stimuli. *C. jejuni* is a host-associated organism that infects various animals and humans and can survive long periods under aerobic conditions (59). In contrast to *H. pylori*, *C. jejuni* has a branched electron transport chain with multiple enzymes that utilize more molecules as electron donors and acceptors than *H. pylori* (20). *C. jejuni* genome size is similar to *H. pylori*; however, the number of *C. jejuni* genes encoding regulatory proteins is higher and reflects the broader spectrum of ecological niches inhabited by this bacterium. Consequently, the number of regulatory proteins controlling energy conversion is higher than that in *H. pylori*, with RacRS, LysR (Cj1000), CsrA, and CprRS playing the most significant roles [for details, see reviews (11, 13–15)]. Depending on growth conditions, particularly the availability of electron donors and acceptors, LysR, RacRS, and CprRS regulate the expression of fumarate respiration genes, which is an excellent example of a cross-talk between regulators controlling the same pathways via transcriptional control over the same genes (e.g., *aspA*, *dcuA*, *mfr*, or *frd*) (51, 60, 61). RNA-binding CsrA, a homolog of *E. coli* carbon starvation regulator, is an example of post-transcriptional energy conservation regulation in *C. jejuni*, including control of expression of TCA and ETC genes (62). *A. butzleri* can lead anaerobic, microaerophilic, and aerobic lifestyles as an environmental or animal- and human-associated bacterium. As a generalist, it utilizes many electron donors and acceptors using an electron transport chain similar to those used by the free-living marine *Campylobacterota* (20). *A. butzleri*'s genome encodes many signal transduction proteins (see Introduction), including extracytoplasmic sigma factors (ECF) to adapt to different conditions. However, hardly anything is known about the regulation of *A. butzleri* energy conversion except that a few species of ECFσ impact electron and carbon metabolism by affecting the transcription of genes from carbon metabolism pathways and electron acceptor complexes (10). However, one can expect the highest complexity and speciation of *A. butzleri*'s regulatory circuits, including energy conservation, of all three species.

CemR regulators are highly conserved *Campylobacteria* regulators. However, the molecular mechanism of signal perception by CemR is still enigmatic and cannot be predicted by analogy. Transcriptional regulatory proteins may sense respiration status, the concentrations of electron donors or acceptors, or respiration byproducts (63). We have shown that cysteine residues of HpCemR become oxidized under O_2-triggered oxidative stress *in vivo* and *in vitro*, which changes the protein's DNA-binding activity possibly by structural changes of DNA-protein complex rather than on-off mechanism (24, 26). Recent studies on CjCemR interactions with the promoter region of *lctP* suggested a similar mechanism of CjCemR activity control and *lctP* transcription regulation (27). AbCemR protein also contains cysteine residues, one of which is conserved in all three species (C27 in HpCemR and CjCemR, C31 in AbCemR). The mechanism of activity regulation by the redox state of the cysteine residues resembles that of ArcA-ArcB two-component system regulation. However, in that TCS, the cysteine residues of ArcB sensor kinase are oxidated, triggering autophosphorylation of ArcB, while ArcA response regulator is activated by phosphorylation. CemR proteins are orphan atypical response regulators in which the same molecule receives and executes the signal. Thus, despite some biochemical similarity to ArcAB system activation, the exact molecular mechanism of CemR activity control has not yet been discovered.

In summary, CemR, the global regulatory protein, is a part of the cell response to a metabolic redox imbalance either caused by environmental conditions such as oxygen availability or ROS or triggered intracellularly due to metabolic changes and increased ROS production. However, the exact pathway of signal transduction by CemR and the levels or hierarchy of regulation are still unknown. Further comprehensive, multi-omic studies are needed to reveal the complex circuits of regulation involving CemR and other regulatory proteins in *Campylobacteria* energy conservation.

MATERIALS AND METHODS

Materials and culture conditions

The strains, plasmids, and proteins used in this work are listed in the Table S1. The primers used in this study are listed in Table S2. *C. jejuni* and *A. butzleri* plate cultures were grown on Columbia blood agar base medium supplemented with 5% defibrinated sheep blood (CBA-B). The liquid cultures were prepared in brain heart infusion broth (BHI) (Oxoid) and incubated with 140-rpm orbital shaking. All *C. jejuni* and *A. butzleri* cultures were supplemented with antibiotic mixes [*C. jejuni*: vancomycin (5 µg/mL), polymyxin B (2.5 U/mL), trimethoprim (5 µg/mL), and amphotericin B (4 µg/mL) (64); *A. butzleri*: cefoperazone (8 µg/mL), amphotericin (10 µg/mL), and teicoplanin (4 µg/mL) (65)]. If necessary for selecting mutants, appropriate antibiotics were used with the following final concentrations: (i) kanamycin 20 µg/mL (*C. jejuni* and *A. butzleri*) and (ii) chloramphenicol 8 µg/mL (*C. jejuni*). Routinely, *C. jejuni* and *A. butzleri* were cultivated at 42°C or 30°C, respectively, under optimal microaerobic conditions (*C. jejuni*: 5% O_2, 8% CO_2, 4% H_2, and 83% N_2; *A. butzleri*: 6% O_2, 9% CO_2, and 85% N_2) generated by the jar evacuation-replacement method using Anaerobic Gas System PetriSphere. The gas mixtures were modified by lowering or increasing O_2 and H_2 concentrations for ATP assays and growth curve analyses. Briefly, bacteria were cultured under microaerobic conditions optimal for each species to the late logarithmic growth phase (OD_{600} ~0.8), diluted to an OD_{600} of ~0.05 and incubated under the desired atmosphere as long as required, up to OD_{600} = 0.2–0.6 for ATP and RT-qPCR or until late stationary phase in growth analyses. The gas mixture with or without H_2 was composed of optimal gas mixtures for *C. jejuni* and *A. butzleri*, respectively. Low oxygen gas mixture was composed of 1% O_2, 10% CO_2, 5% H_2, and 84% N_2, while high oxygen gas mixture was composed of 10% O_2, 5% CO_2, 3% H_2, and 82% N_2. *Escherichia coli* DH5α and BL21 were used for cloning and recombinant protein synthesis. If necessary for selecting *E. coli*, appropriate antibiotics were used with he following final concentrations: (i) kanamycin 50 µg/mL and (ii) ampicillin 100 µg/mL.

Construction of *C. jejuni* mutant strains

C. jejuni mutant strains were constructed using a homologous recombination and natural transformation approach (66). *C. jejuni* NCTC 11168 was grown in 12-mL BHI to an OD_{600} = 0.2. Next, 150 µL of the culture was centrifuged and resuspended in fresh 150 µL of BHI. One hundred fifty nanograms (1 µg/mL) of EcoRI methylated plasmid was added to the culture and cultivated at 42°C in microaerobic (5% O_2, 8% CO_2, 4% H_2, and 83% N_2) conditions with shaking (140 rpm) for 4 h. Next, 100 µL was spread on CBA-B plates with an appropriate antibiotic and incubated for 3 days at 42°C under microaerobic (5% O_2, 8% CO_2, 4% H_2, and 83% N_2) conditions.

C. jejuni NCTC 11168 ΔCj1608

The *C. jejuni Cj1608* deletion construct (pCR2.1/ΔCj1608) was prepared as follows (Fig. S11A). The upstream and downstream regions of *Cj1608* were amplified by PCR using the P1-P2 and P5-P6 primer pairs, respectively, and a *C. jejuni* NCTC 11168 genomic DNA as a template. The *aphA-3* cassette was amplified using the P3-P4 primer pair; pTZ57R/TΔHP1021 (23) was used as a template. The resulting fragments were purified on an agarose gel. Subsequently, the fragments were combined into one DNA amplicon with an overlap extension PCR reaction using the P1-P6 primers. The generated amplicon was purified on an agarose gel and cloned to the pCR2.1-TOPO plasmid (Thermo Fisher Scientific) according to the manufacturer's protocol. The DNA fragment cloned in pCR2.1-TOPO was sequenced. Subsequently, *C. jejuni* NCTC 11168 was transformed with the pCR2.1/ΔCj1608 plasmid, and the transformants were selected by plating on CBA-B plates supplemented with kanamycin. The addition of hydrogen was necessary to obtain the kanamycin-resistant colonies. The allelic exchange was verified by PCR using

the P7-P8 primer pair. The lack of *Cj1608 in C. jejuni* NCTC 11168 ΔCj1608 was confirmed by RNA-seq (Fig. S11B), LC-MS/MS (S1 Data), and Western blot (Fig. S11C and D).

C. jejuni NCTC 11168 C_{Cj1608}

The *C. jejuni Cj1608* complementation construct (pUC18/COMCj1608) was prepared as follows (Fig. S11A). The regions upstream and downstream of the *Cj1608* gene were amplified by PCR using the P1-P6 primer pair and *C. jejuni* Cj1608 genomic DNA as a template. The resulting fragment was purified on an agarose gel. Subsequently, the generated amplicon and the SmaI digested vector pUC18 were ligated according to the method described by Gibson et al. (67) to give pUC18/COMCj1608. *E. coli* DH5α competent cells were transformed with the construct by heat shock. The insert cloned into pUC18 was sequenced. The pUC18/COMCj1608 was used to complement the lack of *Cj1608* in *C. jejuni* NCTC 11168 ΔCj1608 by an attempt similar to Multiplex Genome Editing by Natural Transformation (MuGENT) (68). For the selection, a pSB3021 suicide plasmid was used. The plasmid harbors a *cat* cassette flanked by arms of homology, enabling *cat* cassette integration into the *hsdM* gene. Subsequently, the obtained pUC18/COMCj1608 (1 µg/mL) and pSB3021 (0.25 µg/mL) plasmids were used in the natural transformation of *C. jejuni* NCTC 11168 ΔCj1608. The transformants were selected by plating on CBA-B plates supplemented with chloramphenicol. The bacteria were cultured without hydrogen to increase the selection process. The allelic exchange was verified by PCR using the P7-P9 primers. The presence of *Cj1608* in *C. jejuni* NCTC 11168 $C_{Cj1608}$was confirmed by RNA-seq (Fig. S11B), LC-MS/MS (S1 Data), and Western blot (Fig. S10C and D).

Construction of *A. butzleri* mutant strain

A. butzleri RM4018 mutant strain was constructed using a homologous recombination and electroporation approach. *A. butzleri* was grown in 25-mL BHI to an OD_{600} = 0.4. Next, the culture was transferred on ice and left for 10 min, then centrifuged (4,700 g, 10 min, 4°C) and washed twice with 20 mL of ice-cold glycerine water (15% glycerol and 7% sucrose, filtrated). Finally, the culture was suspended in 250 µL of ice-cold glycerine water. For electroporation, 50 µL of electrocompetent cells was mixed with 5 µg of appropriate plasmid. Electroporation was performed in 0.1-cm electroporation cuvettes (The Cell Projects) using a Gene Pulser II Electroporator (Bio-Rad) using the following parameters: 12.5 kV/cm, 200 Ω, and 25 µF. Cells were regenerated by adding 1 mL of BHI medium to the cuvette, then by transferring the cells to a flask with 2-mL BHI and cultivated with shaking (140 rpm) for 4 h at 30°C in microaerobic conditions. Next, the culture was centrifuged (4,700 g, 10 min, 22°C), resuspended in 100 µL of BHI, spread on CBA-B plates with appropriate antibiotic, and incubated for 5 days at 30°C under microaerobic conditions.

A. butzleri RM4018 ΔAbu0127

The *A. butzleri Abu0127* deletion construct (pUC18/ΔAbu0127) was prepared as follows (Fig. S12A) (69). The upstream and downstream regions of *Abu0127* were amplified by PCR using the P10-P11 and P14-P15 primer pairs, respectively, and an *A. butzleri* RM4018 genomic DNA as a template. The *aphA-3* cassette was amplified using the P12-P13 primer pair; pTZ57R/TΔHP1021 (23) was used as a template. The resulting fragments were purified on an agarose gel. Subsequently, the PCR-amplified fragments and the SmaI digested vector pUC18 were ligated according to the method of Gibson et al. (67). Subsequently, *A. butzleri* RM4018 was transformed via electroporation with the pUC18/ΔAbu0127 plasmid, and the transformants were selected by plating on CBA-B plates supplemented with kanamycin. The allelic exchange was verified by PCR using the P16-P17 primer pair. The lack of *Abu0127* in *A. butzleri* RM4018 ΔAbu0127 was confirmed by RNA-seq (Fig. S12B), LC-MS/MS (S2 Data), and Western blot (Fig. S12C and D).

Disk diffusion assay

Bacteria were cultured in BHI to OD_{600} = ~0.5 to 0.7 and then diluted to OD_{600} = 0.1 in BHI. Each culture was spread by a cotton swab on CBA-B plates. Sterile, glass fiber 6-mm disks were placed on plates, and 5 µL of tested solutions were dropped on disks: 2% H_2O_2 (POCH, 885193111), 2% paraquat dichloride (Acros Organics, 227320010), 5% hydroxyurea (Merck, H8627-1G), 3% sodium nitroprusside (Merck, S0501), 2.5% menadion (Merck, A13593), and 15% sodium hypochlorite (Merck, 1056142500). Sodium hypochlorite solutions for assays were made fresh; the solutions' pH was adjusted by adding HCl to pH 7 and kept in phosphate-buffered saline (PBS) buffer prior to experiments (70). Menadion solution was prepared in dimethyl sulfoxide (DMSO). The diameter of the inhibition zone around the disks was determined after 3 days of incubation under microaerobic conditions. The experiment was performed using three biological replicates.

RNA isolation

Bacterial cultures (12-mL BHI) of *C. jejuni* and *A. butzleri* strains were grown under microaerobic conditions to OD_{600} of 0.5–0.6. Immediately after opening the jar, 2 mL of the non-stressed culture was added to 2 mL of the RNAprotect Bacteria Reagent (Qiagen), vortexed, and incubated for 5 min at room temperature. In parallel, the cultures were treated with 1-mM paraquat (final concentration) for 25 min (*C. jejuni* 42°C, *A. butzleri* 30°C, 140-rpm orbital shaking). After oxidative stress, samples were collected similarly to non-stressed cells. After 5-min incubation with RNAprotect Bacteria Reagent, bacteria were collected by centrifugation (4,700 × *g*, 10 min, room temperature). RNA was isolated by GeneJET RNA Purification Kit (Thermo Fisher Scientific, K0731) according to the manufacturer's protocol and treated with RNase-free DNase I (Thermo Fisher Scientific). Next, purification by the GeneJET RNA Purification Kit was performed to remove DNase I. A NanoDrop Lite spectrophotometer, agarose gel electrophoresis, and Agilent 4200 TapeStation System were used to determine the RNA quality and quantity. RNA was isolated immediately after bacteria collection, stored at −80°C for up to 1 month and used for RNA sequencing. RNA was isolated from three independent cultures.

For analyses of gene transcription dependent on oxygen supply, bacterial cells were collected from cultures under the logarithmic phase of growth (OD_{600} ~0.2 to 0.5), grown under the desired atmosphere (see Materials and Culture Conditions), and RNA was isolated as described above.

RNA-seq

Preparation and sequencing of the prokaryotic directional mRNA library were performed at the Novogene Bioinformatics Technology Co. Ltd. (Cambridge, UK). Briefly, the ribosomal RNA was removed from the total RNA, followed by ethanol precipitation. After fragmentation, the first strand of cDNA was synthesized using random hexamer primers. During the second-strand cDNA synthesis, deoxyuridine triphosphates were replaced with deoxythymidine triphosphates in the reaction buffer. The directional library was ready after end repair, A-tailing, adapter ligation, size selection, USER enzyme digestion, amplification, and purification. The library was checked with Qubit, RT-qPCR for quantification, and a bioanalyzer for size distribution detection. The libraries were sequenced with the NovaSeq 6000 (Illumina), and 150-bp reads were produced.

RNA-seq analysis

The 150-bp paired reads were mapped to the *C. jejuni* NCTC 11168 (NC_002163.1) or *A. butzleri* RM4018 (NC_009850.1) genome depending on the species analyzed using Bowtie2 software with local setting (version 2.3.5.1) (71, 72) and processed using samtools (version 1.10) (73), achieving more than 10^6 mapped reads on average. Differential analysis was performed using R packages Rsubread (version 2.10) and edgeR (version 3.38) (74, 75), following a protocol described in reference (76). Genes rarely

transcribed were removed from the analysis (less than 10 mapped reads per library). The obtained count data were normalized using the edgeR package, and a quasi-likelihood negative binomial was fitted. Differential expression was tested using the glmTtreat function with a 1.45-fold change (FC) threshold. Only genes with a false discovery rate (FDR) less than 0.05 and $|\log_2 FC|$ of ≥ 1 were considered differentially expressed. Data visualization with volcano plots was done using the EnhancedVolcano and tidyHeatmap R packages (versions 1.14 and 1.8.1) (77). The reproducibility of *C. jejuni* and *A. butzleri* biological replicates was visualized by principal component analysis (PCA) of the normalized RNA-seq CPM data (Fig. S13A and B).

Proteomic sample preparation

Bacterial cultures of wild-type *C. jejuni* NCTC 11168 and *A. butzleri* RM4018 strains and their isogenic mutant strains, ΔCj1608 or ΔAbu0127, respectively, were grown in BHI under microaerobic conditions to an OD_{600} of 0.5–0.7 and split into two subcultures of 10 mL each. The first subculture was harvested, washed, and lysed immediately after opening the jar; the second subculture (only WT strains) was harvested, washed, and lysed after incubation with 1-mM paraquat (*C. jejuni*: 42°C, *A. butzleri*: 30°C, with orbital shaking at 140 rpm) for 30 and 60 min. The bacterial proteomes were prepared as described previously by Abele et al. (78). Briefly, cells were harvested by centrifugation at 10,000 × *g* for 2 min; media were removed; and cells were washed once with 20 mL of 1 × PBS. The cell pellets were suspended and lysed in 100 µL of 100% trifluoroacetic acid (Roth) (79) for 5 min at 55°C. Next, 900 µL of neutralization buffer (2-M Tris) was added and vortexed. Protein concentration was measured using Bradford assay (Bio-Rad). Fifty micrograms of protein per sample was reduced [9-mM tris(2-carboxyethyl)phosphine] and carbamidomethylated (40 mM chloroacetamide) for 5 min at 95°C. The proteins were digested by adding trypsin (proteomics grade, Roche) at a 1:50 enzyme:protein ratio (wt/wt) and incubation at 37°C overnight. Digests were acidified by the addition of 3% (vol/vol) formic acid (FA) and desalted using self-packed StageTips (five disks per microcolumn, ø 1.5 mm, C18 material; 3M Empore). The peptide eluates were dried to completeness and stored at −80°C. Before the LC-MS/MS measurement, all samples were freshly resuspended in 12-µL 0.1% FA in high-performance liquid chromatography (HPLC)-grade water, and around 25 µg of total peptide amount was injected into the mass spectrometer per measurement. Each experiment was performed using four biological replicates.

Proteomic data acquisition and data analysis

Peptides were analyzed on a Vanquish Neo liquid chromatography system (microflow configuration) coupled to an Orbitrap Exploris 480 mass spectrometer (Thermo Fisher Scientific). Around 25 µg of peptides was applied onto an Acclaim PepMap 100 C18 column (2-µm particle size, 1-mm ID × 150 mm, 100-Å pore size; Thermo Fisher Scientific) and separated using a two-step gradient. In the first step, a 50-min linear gradient ranging from 3% to 24% solvent B (0.1% FA, 3% DMSO in acetonitrile) in solvent A (0.1% FA and 3% DMSO in HPLC-grade water) at a flow rate of 50 µL/min was applied. In the second step, solvent B was further increased from 24% to 31% over a 10-min linear gradient. The mass spectrometer was operated in data-dependent acquisition and positive ionization modes. MS1 full scans (360–1,300 *m/z*) were acquired with a resolution of 60,000, a normalized automatic gain control (AGC) target value of 100%, and a maximum injection time of 50 ms. Peptide precursor selection for fragmentation was carried out using a fixed cycle time of 1.2 s. Only precursors with charge states from 2 to 6 were selected, and dynamic exclusion of 30 s was enabled. Peptide fragmentation was performed using higher-energy collision-induced dissociation and a normalized collision energy of 28%. The precursor isolation window width of the quadrupole was set to 1.1 *m/z*. MS2 spectra were acquired with a resolution of 15,000, a fixed first mass of 100 *m/z*, a normalized AGC target value of 100%, and a maximum injection time of 40 ms.

Peptide identification and quantification were performed using MaxQuant (version 1.6.3.4) with its built-in search engine Andromeda (80, 81). MS2 spectra were searched against the *C. jejuni or A. butzleri* proteome database derived from *C. jejuni* NCTC 11168 (NC_002163.1) or *A. butzleri* RM4018 (NC_009850.1), respectively. Trypsin/P was specified as the proteolytic enzyme. The precursor tolerance was set to 4.5 ppm, and fragment ion tolerance was set to 20 ppm. Results were adjusted to a 1% FDR on peptide spectrum match level and protein level employing a target-decoy approach using reversed protein sequences. The minimal peptide length was defined as seven amino acids; carbamidomethylated cysteine was set as fixed modification and oxidation of methionine and N-terminal protein acetylation as variable modifications. The match-between-run function was disabled. Protein abundances were calculated using the label-free quantification (LFQ) algorithm from MaxQuant (82). Protein intensity values were logarithm transformed (base 2), and a Student *t*-test was used to identify proteins differentially expressed between conditions. The resulting *P* values were adjusted by the Benjamini-Hochberg algorithm (83) to control the FDR. Since low abundant proteins are more likely to result in missing values, we filled in missing values with a constant of half the lowest detected LFQ intensity per protein. However, if the imputed value was higher than the 20% quantile of all LFQ intensities in that sample, we used the 20% quantile as the imputed value. Only proteins with $|\log_2 FC|$ of ≥ 1 were considered differentially expressed (84).

The reproducibility of *C. jejuni* and *A. butzleri* biological replicates was visualized by PCA of the normalized LC-MS/MS CPM data (Fig. S13C and D).

Omics data analysis

The KEGG (85) gene/protein set enrichment analysis of the differentially expressed genes and proteins was performed and visualized based on the clusterProfiler (29) (version 4.8.2) package in R software with a *P* value of < 0.05. Genome-wide functional annotation was carried out with the eggNOG-mapper (version 5.0) (86) according to the COG database (87) with an *e* value of 0.001 and a minimum hit bit score of 60. Visual representations of RNA expression levels and LC-MS/MS expressed proteins in different COGs were performed with the Circos Table viewer (http://mkweb.bcgsc.ca/tableviewer/, accessed on 5 November 2023). For the analyses, only genes and proteins with a $|\log_2 FC|$ of ≥ 1 and an FDR of < 0.05 were considered as significantly changed.

ChIP

Bacterial cultures (70- mL BHI) of *C. jejuni* NTCT 11168 and *A. butzleri* RM4018 wild-types and ΔCj1608 and Abu0127 mutants were grown to an OD_{600} of 0.5–0.7. The culture was cross-linked with 1% formaldehyde for 5 min immediately after opening the jar. The cross-linking reactions were stopped by treatment with 125 mM glycine for 10 min at room temperature. The cultures were centrifuged at 4,700 × *g* for 10 min at 4°C and washed twice with 25 mL of ice-cold 1 × PBS, followed by the same centrifugation step. Samples were resuspended in 1.1- mL immunoprecipitation (IP) buffer (150-mM NaCl, 50-mM Tris-HCl, pH 7.5, 5-mM EDTA, 0.5% vol/vol NP-40, and 1.0% vol/vol Triton X-100) and sonicated [Ultraschallprozessor UP200s (0.6%/50% power, 30-s on, 0-s off, ice bucket)] to reach a 100- to 500-bp DNA fragment size. Next, the samples were centrifuged at 12,000 × *g* for 10 min at 4°C. One hundred microliters of the supernatant was used for input preparation. Nine hundred microliters of the supernatant was incubated with 30 µL of Sepharose Protein A (Rockland, PA50-00-0002) (pre-equilibrated in IP buffer) for 1 h at 4°C on a rotation wheel. The samples were centrifuged at 1,000 × *g* for 2 min at 4°C. The supernatants were incubated with 100-µL antibody-Sepharose A complex (see below) and incubated at 4°C for 24 h on a rotation wheel. Next, the samples were centrifuged at 1,000 × *g* for 2 min at 4°C, and the supernatant was discarded. The beads were washed four times with IP-wash buffer (50-mM Tris-HCl, pH 7.5, 150-mM NaCl, 0.5% NP-40, 0.1% SDS), twice with Tris-EDTA (TE) buffer (10-mM Tris-HCl, pH 8.0; 0.1-mM EDTA), resuspended in 180 µL of TE buffer, and treated with 20-µg/mL RNase A at

37°C for 30 min. Next, cross-links were reversed by adding sodium dodecyl sulfate (SDS) at a final concentration of 0.5% and proteinase K at a final concentration of 20 µg/mL, followed by incubation for 16 h at 37°C. The beads were removed by centrifugation at 1,000 × *g* for 2 min at 4°C, and the DNAs from the supernatants were isolated with ChIP DNA Clean & Concentrator (Zymo Research). The quality of DNA was validated by electrophoresis in 2% agarose gel, and the concentration was determined with QuantiFluor dsDNA System (Promega). The ChIP-DNA was isolated from three independent bacteria cultures.

The *C. jejuni* antibody-Sepharose A complex was prepared by adding 40 µg of desalted rabbit polyclonal anti-Cj1608 antibody to 100 µL of the Sepharose Protein A pre-equilibrated in IP buffer. *A. butzleri* antibody-sepharose A complex was prepared by adding 120 µg of desalted rabbit polyclonal anti-Abu0127 antibody to 100 µL of the Sepharose Protein A pre-equilibrated in IP buffer. The binding reaction was performed on a rotation wheel for 24 h at 4°C. Next, the complex was washed five times with an IP buffer. The antibodies used in ChIP were raised in rabbits and validated with Western blot (Fig. S11D and D).

Quantitative polymerase chain reaction

RT-qPCR quantified the mRNA levels of the selected genes. The reverse transcription was conducted using 500 ng of RNA in a 20-µL volume reaction mixture of iScript cDNA Synthesis Kit (Bio-Rad). Diluted cDNA (1:10, 2.5 µL) was added to 7.5 µL of Sensi-FAST SYBR No-ROX (Bioline) and 400 nM of forward and reverse primers in a 15-µL final volume. The RT-qPCR program was 95°C for 3 min, followed by 40 three-step amplification cycles consisting of 5 s at 95°C, 10 s at 58°C, and 20 s at 72°C. The following primer pairs were used: P18-P19, *gltA* for *C. jejuni* RT-qPCR, and P23-P24, *nuoB* for *A. butzleri* RT-qPCR (Table S2). The relative quantity of mRNA for each gene of *C. jejuni* was determined by referring to the mRNA levels of *recA* (P25-P26 primer pair). The relative quantity of mRNA for each gene of *A. butzleri* was determined by referring to the mRNA levels of *gyrA* (P27-P28 primer pair). The RT-qPCR was performed for three independent bacterial cultures.

The protein-DNA interactions in the cell *in vivo* of the selected DNA regions were quantified by ChIP-qPCR. Diluted immunoprecipitation output (1:0, 2.5 µL) was added to 7.5 µL of Sensi-FAST SYBR No-ROX (Bioline) and 400 nM of forward and reverse primers in a 15-µL final volume. The ChIP-qPCR was performed using the following program: 95°C for 3 min, followed by 40 three-step amplification cycles consisting of 10 s at 95°C, 10 s at 59°C, and 20 s at 72°C. The following primer pairs were used: P43-P44, p*gltA* (*C. jejuni*), and P45-P46, p*nuoA* (*A. butzleri*) (Table S2). The *recA* (P25-P26) and *gyrA* (P27-P28) genes were used as a negative control for *C. jejuni* and *A. butzleri*, respectively (Table S2). No-antibody control was used for ChIP-qPCR normalization, and the fold enrichment was calculated. The ChIP-qPCR was performed for three independent bacterial cultures.

The RT-qPCR and ChIP-qPCR were performed using the CFX96 Touch Real-Time PCR Detection Systems, and data were analyzed with CFX Maestro (Bio-Rad) software.

Construction of plasmids expressing recombinant wild-type Cj1608 and Abu0127 proteins

The *Cj1608* (*Cj1509* in *C. jejuni* 81–116) gene (888 bp) was amplified with primer pair P29-P30 using *C. jejuni* 81–116 genomic DNA as a template. The *Abu0127* gene (891 bp) was amplified with primer pair P31-P32 using *A. butzleri* RM4018 genomic DNA as a template. The PCR products were digested with BamHI/SalI and cloned into BamHI/SalI sites of pET28Strep (24) to generate pETStrepCj1509 and pETStrepAbu0127, respectively (Table S1).

Protein expression and purification

The recombinant Strep-tagged Cj1608 (Cj1509 of *C. jejuni* 81–116) and Abu0127 proteins were purified according to the Strep-Tactin manufacturer's protocol (IBA Lifesciences).

Briefly, *E. coli* BL21 cells (1 L) carrying either the pET28/StrepCj1509 or pET28/StrepAbu0127 vectors were grown at 37°C. At an OD_{600} of 0.8, protein synthesis was induced with 0.05-mM IPTG for 3 h at 30°C for Cj1608 and overnight at 18°C for Abu0127. The cultures were harvested by centrifugation (10 min; 5,000 × *g*; at 4°C). The cells were suspended in 20 mL of ice-cold buffer W (100-mM Tris-HCl, pH 8.0; 300-mM NaCl; and 1-mM EDTA) supplemented with cOmplete, EDTA-free protease inhibitor Cocktail (Roche), disrupted by sonication, and centrifuged (30 min; 31,000 × *g*; at 4°C). The supernatant was applied onto a Strep-Tactin Superflow high-capacity Sepharose column (1-mL bed volume, IBA). The column was washed with buffer W until Bradford tests yielded a negative result, and then washed with 5 mL of buffer W without EDTA. The elution was carried out with approximately 6 × 0.8 mL of buffer E (100-mM Tris-HCl, pH 8.0; 300-mM NaCl; and 5-mM desthiobiotin). Protein purity was analyzed by SDS-PAGE electrophoresis using GelDoc XR+ and ImageLab software (Bio-Rad). The fractions were stored at −20°C in buffer E diluted with glycerol to a final concentration of 50%.

EMSA

PCR amplified DNA probes in two steps. DNA fragments were amplified in the first step using unlabeled primer pairs P33-P34 (p*gltA*) and P35-P36 (*recJ*) with a *C. jejuni* NCTC 11168 genomic DNA template, and P37-P38 (p*nuo*) and P39-P40 (*recA*) with an *A. butzleri* RM4018 genomic DNA template (Table S1). The forward primers were designed with overhangs complementary to P41 (FAM labeled) for p*nuo* and p*gltA* and P42 (Cy5 labeled) for *recJ* and *recA*. The unlabeled fragment was purified and used as a template in the second round of PCR using the appropriate fluorophore-labeled primer and the appropriate reverse primer used in the first step. Both fluorophore-labeled DNAs (each 5 nM) were incubated with the Strep-tagged protein at 30°C (Abu0127) or 37°C (Cj1608) for 20 min in Tris buffer (50-mM Tris-HCl, pH 8.0; 100-mM NaCl; and 0.2% Triton X-100). The complexes were separated by electrophoresis on a 4% polyacrylamide gel in 0.5 × Tris-Borate-EDTA (TBE) (1× TBE: 89-mM Tris, 89-mM borate, and 2-mM EDTA) at 10 V/cm in the cold room (approximately 10°C). The gels were analyzed using Typhoon 9500 FLA Imager and ImageQuant software.

ATP assay

The ATP level was measured with the BacTiter-Glo Assay. *C. jejuni and A. butzleri* cultures were grown in the BHI medium to the logarithmic growth phase (OD_{600} of 0.5–0.7). Cells were diluted to an OD_{600} = 0.1 with fresh medium. Next, 50 µL of bacteria was mixed with 50 µL of BacTiter-Glo (Promega) and incubated at room temperature for 5 min. The luminescence was measured with a CLARIOstar plate reader on opaque-walled multi-well plates (SPL Life Sciences, 2–200203). Each experiment was performed using three biological replicates.

Statistics and reproducibility

Statistical analysis was performed using GraphPad Prism (version 8.4.2) and R (version 4.3.1) statistical software. All *in vivo* experiments were repeated at least three times, and data were presented as mean ± SD. The statistical significance between the two conditions was calculated by paired two-tailed Student *t*-test. The statistical significance between multiple groups was calculated by one-way analysis of variance (ANOVA) with Tukey's post hoc test. A *P* value of < 0.05 was considered statistically significant. The proteome and transcriptome correlations were determined with the Pearson correlation coefficient. The EMSA and Western blot experiments were repeated twice with similar results.

ACKNOWLEDGMENTS

We thank Kinga Surmacz for helping with disk diffusion assays, Maria Cieślak for helping with pUC18/ΔAbu0127 plasmid preparation, and Verena Breitner and Tayma Midari for technical assistance at BayBioMS.

This work has been supported by the OPUS 17 (project number 2019/33/B/NZ6/01648, funded by the National Science Centre, Poland, to A.Z.-P.) and by the EPIC-XS (project number 823839, funded by the Horizon 2020 Program of the European Union, to C.L.).

The open-access publication of this article was funded by the OPUS 17 (2019/33/B/NZ6/01648, National Science Centre, Poland) and statutory funds from the Ludwik Hirszfeld Institute of Immunology and Experimental Therapy, Polish Academy of Sciences.

AUTHOR AFFILIATIONS

[1]Department of Microbiology, Hirszfeld Institute of Immunology and Experimental Therapy, Polish Academy of Sciences, Wrocław, Poland
[2]Department of Molecular Microbiology, Faculty of Biotechnology, University of Wrocław, Wrocław, Poland
[3]Department of Biological Safety, Unit of Product Hygiene and Disinfection Strategies, German Federal Institute for Risk Assessment, Berlin, Germany
[4]Bavarian Center for Biomolecular Mass Spectrometry (BayBioMS), Technical University of Munich (TUM), Freising, Germany
[5]Department of Biological Safety, National Reference Laboratory for *Campylobacter*, German Federal Institute for Risk Assessment, Berlin, Germany

AUTHOR ORCIDs

Mateusz Noszka http://orcid.org/0000-0002-6694-1394
Agnieszka Strzałka http://orcid.org/0000-0002-7092-0609
Jakub Muraszko http://orcid.org/0000-0001-7232-0298
Dirk Hofreuter http://orcid.org/0000-0002-2589-9206
Miriam Abele http://orcid.org/0000-0003-0084-2999
Christina Ludwig http://orcid.org/0000-0002-6131-7322
Kerstin Stingl http://orcid.org/0000-0002-8338-717X
Anna Zawilak-Pawlik http://orcid.org/0000-0003-1824-1550

FUNDING

Funder	Grant(s)	Author(s)
Narodowe Centrum Nauki (NCN, National Science Centre, Poland)	OPUS 17 2019/33/B/NZ6/01648	Anna Zawilak-Pawlik
EC | Horizon 2020 Framework Programme (H2020)	EPIC-XS Project Number 823839	Christina Ludwig

AUTHOR CONTRIBUTIONS

Mateusz Noszka, Conceptualization, Data curation, Formal analysis, Funding acquisition, Investigation, Methodology, Validation, Visualization, Writing – original draft, Writing – review and editing, Software, Supervision | Agnieszka Strzałka, Formal analysis, Methodology, Software, Writing – review and editing, Supervision, Investigation, Visualization, Validation | Jakub Muraszko, Investigation, Writing – review and editing | Dirk Hofreuter, Validation, Writing – review and editing, Formal analysis | Miriam Abele, Data curation, Methodology, Writing – review and editing, Validation | Christina Ludwig, Funding acquisition, Methodology, Writing – review and editing | Kerstin Stingl, Conceptualization, Methodology, Writing – review and editing, Formal

analysis, Project administration, Validation | Anna Zawilak-Pawlik, Conceptualization, Formal analysis, Funding acquisition, Project administration, Supervision, Validation, Visualization, Writing – original draft, Writing – review and editing, Data curation

DATA AVAILABILITY

The *Campylobacter jejuni* RNA-seq FASTQ and processed data generated in this study have been deposited in the ArrayExpress database (EMBL-EBI) under accession code E-MTAB-13650. The *Arcobacter butzleri* RNA-seq FASTQ and processed data generated in this study have been deposited in the ArrayExpress database (EMBL-EBI) under accession code E-MTAB-13649. The raw proteomics data, MaxQuant search results, and the used protein sequence database generated in this study have been deposited in the ProteomeXchange Consortium via the PRIDE partner repository (88) under accession code PXD048711. *Campylobacter jejuni* NCTC 11168 reference genome is deposited in the National Center for Biotechnology Information under accession code NC_002163.1. *Arcobacter butzleri* RM4018 reference genome is deposited in the National Center for Biotechnology Information under accession code NC_009850.1. All of the code and data used to generate the figure presented here are deposited in GitHub via https://github.com/NoszkaM/LBMM.git.

ETHICS APPROVAL

The antibodies used in chromatin immunoprecipitation and western blot were raised in rabbits under the approval of the First Local Committee for Experiments with the Use of Laboratory Animals, Wroclaw, Poland (consent number 053/2020/P2).

ADDITIONAL FILES

The following material is available online.

Supplemental Material

Data S1 (mSystems00784-24-s0001.xlsx). Full list of genes and proteins of the Cj1608 regulon.
Data S2 (mSystems00784-24-s0002.xlsx). Full list of genes and proteins of the Abu0127 regulon.
Data S3 (mSystems00784-24-s0003.xlsx). Genes and proteins of selected processes or pathways in *C. jejuni*, *A. butzleri*, and *H. pylori*.
Supplemental material (mSystems00784-24-s0004.pdf). Figures S1 to S13, Tables S1 and S2, and descriptions of Data S1 to S3.

Open Peer Review

PEER REVIEW HISTORY (review-history.pdf). An accounting of the reviewer comments and feedback.

REFERENCES

1. Waite DW, Chuvochina MS, Hugenholtz P. 2019. Road map of the phylum *Campylobacterota*, p 1–11. In Bergey's manual of systematics of archaea and bacteria
2. Chieffi D, Fanelli F, Fusco V. 2020. *Arcobacter butzleri*: up-to-date taxonomy, ecology, and pathogenicity of an emerging pathogen. Compr Rev Food Sci Food Saf 19:2071–2109. https://doi.org/10.1111/1541-4337.12577
3. Burnham PM, Hendrixson DR. 2018. *Campylobacter jejuni*: collective components promoting a successful enteric lifestyle. Nat Rev Microbiol 16:551–565. https://doi.org/10.1038/s41579-018-0037-9
4. Shange N, Gouws P, Hoffman LC. 2019. *Campylobacter* and *Arcobacter* species in food-producing animals: prevalence at primary production and during slaughter. World J Microbiol Biotechnol 35:146. https://doi.org/10.1007/s11274-019-2722-x
5. Tacconelli E, Carrara E, Savoldi A, Harbarth S, Mendelson M, Monnet DL, Pulcini C, Kahlmeter G, Kluytmans J, Carmeli Y, et al. 2018. Discovery, research, and development of new antibiotics: the WHO priority list of antibiotic-resistant bacteria and tuberculosis. Lancet Infect Dis 18:318–327. https://doi.org/10.1016/S1473-3099(17)30753-3
6. Sciortino S, Arculeo P, Alio V, Cardamone C, Nicastro L, Arculeo M, Alduina R, Costa A. 2021. Occurrence and antimicrobial resistance of *Arcobacter* spp. recovered from aquatic environments. Antibiotics (Basel) 10:288. https://doi.org/10.3390/antibiotics10030288
7. Gumerov VM, Ulrich LE, Zhulin IB. 2024. MiST 4.0: a new release of the microbial signal transduction database, now with a metagenomic

component. Nucleic Acids Res 52:D647–D653. https://doi.org/10.1093/nar/gkad847
8. Gundogdu O, Bentley SD, Holden MT, Parkhill J, Dorrell N, Wren BW. 2007. Re-annotation and re-analysis of the *Campylobacter jejuni* NCTC11168 genome sequence. BMC Genomics 8:1–8. https://doi.org/10.1186/1471-2164-8-162
9. Miller WG, Parker CT, Rubenfield M, Mendz GL, Wösten M, Ussery DW, Stolz JF, Binnewies TT, Hallin PF, Wang G, Malek JA, Rogosin A, Stanker LH, Mandrell RE. 2007. The complete genome sequence and analysis of the epsilonproteobacterium *Arcobacter butzleri*. PLoS One 2:e1358. https://doi.org/10.1371/journal.pone.0001358
10. Martinez-Malaxetxebarria I, Muts R, van Dijk L, Parker CT, Miller WG, Huynh S, Gaastra W, van Putten JPM, Fernandez-Astorga A, Wösten MMSM. 2012. Regulation of energy metabolism by the extracytoplasmic function (ECF) σ factors of *Arcobacter butzleri*. PLoS One 7:e44796. https://doi.org/10.1371/journal.pone.0044796
11. Gahamanyi N, Song DG, Mboera LEG, Matee MI, Mutangana D, Amachawadi RG, Komba EVG, Pan CH. 2022. Insights into the virulence of *Campylobacter jejuni* associated with two-component signal transduction systems and single regulators. Microbiol Res 13:188–200. https://doi.org/10.3390/microbiolres13020016
12. Chandrashekhar K, Kassem II, Rajashekara G. 2017. *Campylobacter jejuni* transducer like proteins: chemotaxis and beyond. Gut Microbes 8:323–334. https://doi.org/10.1080/19490976.2017.1279380
13. Casado J, Lanas Á, González A. 2022. Two-component regulatory systems in *Helicobacter pylori* and *Campylobacter jejuni*: attractive targets for novel antibacterial drugs. Front Cell Infect Microbiol 12:977944. https://doi.org/10.3389/fcimb.2022.977944
14. Taylor AJ, Kelly DJ. 2019. The function, biogenesis and regulation of the electron transport chains in *Campylobacter jejuni*: new insights into the bioenergetics of a major food-borne pathogen. Adv Microb Physiol 74:239–329. https://doi.org/10.1016/bs.ampbs.2019.02.003
15. Flint A, Stintzi A, Saraiva LM. 2016. Oxidative and nitrosative stress defences of *Helicobacter* and *Campylobacter* species that counteract mammalian immunity. FEMS Microbiol Rev 40:938–960. https://doi.org/10.1093/femsre/fuw025
16. Shan Y, Lai Y, Yan A. 2012. Metabolic reprogramming under microaerobic and anaerobic conditions in bacteria. Subcell Biochem 64:159–179. https://doi.org/10.1007/978-94-007-5055-5_8
17. Imlay JA. 2019. Where in the world do bacteria experience oxidative stress? Environ Microbiol 21:521–530. https://doi.org/10.1111/1462-2920.14445
18. Espey MG. 2013. Role of oxygen gradients in shaping redox relationships between the human intestine and its microbiota. Free Radic Biol Med 55:130–140. https://doi.org/10.1016/j.freeradbiomed.2012.10.554
19. van der Stel A-X, van de Lest CHA, Huynh S, Parker CT, van Putten JPM, Wösten MMSM. 2018. Catabolite repression in *Campylobacter jejuni* correlates with intracellular succinate levels. Environ Microbiol 20:1374–1388. https://doi.org/10.1111/1462-2920.14042
20. van der Stel A-X, Wösten MMSM. 2019. Regulation of respiratory pathways in *Campylobacterota*: a review. Front Microbiol 10:1719. https://doi.org/10.3389/fmicb.2019.01719
21. Ravcheev DA, Gerasimova AV, Mironov AA, Gelfand MS. 2007. Comparative genomic analysis of regulation of anaerobic respiration in ten genomes from three families of gamma-proteobacteria (Enterobacteriaceae, Pasteurellaceae, Vibrionaceae). BMC Genomics 8:1–17. https://doi.org/10.1186/1471-2164-8-54
22. Tomb JF, White O, Kerlavage AR, Clayton RA, Sutton GG, Fleischmann RD, Ketchum KA, Klenk HP, Gill S, Dougherty BA, et al. 1997. The complete genome sequence of the gastric pathogen *Helicobacter pylori*. Nature 388:539–547. https://doi.org/10.1038/41483
23. Donczew R, Makowski Ł, Jaworski P, Bezulska M, Nowaczyk M, Zakrzewska-Czerwińska J, Zawilak-Pawlik A. 2015. The atypical response regulator HP1021 controls formation of the *Helicobacter pylori* replication initiation complex. Mol Microbiol 95:297–312. https://doi.org/10.1111/mmi.12866
24. Szczepanowski P, Noszka M, Żyła-Uklejewicz D, Pikuła F, Nowaczyk-Cieszewska M, Krężel A, Stingl K, Zawilak-Pawlik A. 2021. HP1021 is a redox switch protein identified in *Helicobacter pylori*. Nucleic Acids Res 49:6863–6879. https://doi.org/10.1093/nar/gkab440
25. Pflock M, Bathon M, Schär J, Müller S, Mollenkopf H, Meyer TF, Beier D. 2007. The orphan response regulator HP1021 of *Helicobacter pylori* regulates transcription of a gene cluster presumably involved in acetone metabolism. J Bacteriol 189:2339–2349. https://doi.org/10.1128/JB.01827-06
26. Noszka M, Strzałka A, Muraszko J, Kolenda R, Meng C, Ludwig C, Stingl K, Zawilak-Pawlik A. 2023. Profiling of the *Helicobacter pylori* redox switch HP1021 regulon using a multi-omics approach. Nat Commun 14:6715. https://doi.org/10.1038/s41467-023-42364-6
27. Sinha R, LeVeque RM, Callahan SM, Chatterjee S, Stopnisek N, Kuipel M, Johnson JG, DiRita VJ. 2024. Gut metabolite L-lactate supports *Campylobacter jejuni* population expansion during acute infection. Proc Natl Acad Sci U S A 121:e2316540120. https://doi.org/10.1073/pnas.2316540120
28. Jaworski P, Donczew R, Mielke T, Weigel C, Stingl K, Zawilak-Pawlik A. 2018. Structure and function of the *Campylobacter Jejuni* Chromosome replication origin. Front Microbiol 9:1533. https://doi.org/10.3389/fmicb.2018.01533
29. Wu T, Hu E, Xu S, Chen M, Guo P, Dai Z, Feng T, Zhou L, Tang W, Zhan L, Fu X, Liu S, Bo X, Yu G. 2021. clusterProfiler 4.0: a universal enrichment tool for interpreting omics data. Innovation 2:100141. https://doi.org/10.1016/j.xinn.2021.100141
30. Li S, Lam J, Souliotis L, Alam MT, Constantinidou C. 2022. Posttranscriptional regulation in response to different environmental stresses in *Campylobacter jejuni*. Microbiol Spectr 10:e0020322. https://doi.org/10.1128/spectrum.00203-22
31. Sharma CM, Hoffmann S, Darfeuille F, Reignier J, Findeiss S, Sittka A, Chabas S, Reiche K, Hackermüller J, Reinhardt R, Stadler PF, Vogel J. 2010. The primary transcriptome of the major human pathogen *Helicobacter pylori*. Nature 464:250–255. https://doi.org/10.1038/nature08756
32. Flint A, Stintzi A. 2015. Cj1386, an atypical hemin-binding protein, mediates hemin trafficking to KatA in *Campylobacter jejuni*. J Bacteriol 197:1002–1011. https://doi.org/10.1128/JB.02346-14
33. Fasnacht M, Polacek N. 2021. Oxidative stress in bacteria and the central dogma of molecular biology. Front Mol Biosci 8:671037. https://doi.org/10.3389/fmolb.2021.671037
34. Zhu M, Dai X. 2020. Bacterial stress defense: the crucial role of ribosome speed. Cell Mol Life Sci 77:853–858. https://doi.org/10.1007/s00018-019-03304-0
35. Stahl M, Butcher J, Stintzi A. 2012. Nutrient acquisition and metabolism by *Campylobacter jejuni*. Front Cell Infect Microbiol 2:5. https://doi.org/10.3389/fcimb.2012.00005
36. Surmacz K. 2022. Analysis of *Aliarcobacter butzleri* RM4018 sensitivity to oxidative stress. Wroclaw University of Science and Technology.
37. Zhu M, Dai X. 2019. Maintenance of translational elongation rate underlies the survival of *Escherichia coli* during oxidative stress. Nucleic Acids Res 47:7592–7604. https://doi.org/10.1093/nar/gkz467
38. Benoit SL, Maier RJ, Sawers RG, Greening C. 2020. Molecular hydrogen metabolism: a widespread trait of pathogenic bacteria and protists. Microbiol Mol Biol Rev 84:e00092-19. https://doi.org/10.1128/MMBR.00092-19
39. Guccione EJ, Kendall JJ, Hitchcock A, Garg N, White MA, Mulholland F, Poole RK, Kelly DJ. 2017. Transcriptome and proteome dynamics in chemostat culture reveal how *Campylobacter jejuni* modulates metabolism, stress responses and virulence factors upon changes in oxygen availability. Environ Microbiol 19:4326–4348. https://doi.org/10.1111/1462-2920.13930
40. Kiehlbauch JA, Brenner DJ, Nicholson MA, Baker CN, Patton CM, Steigerwalt AG, Wachsmuth IK. 1991. *Campylobacter butzleri* sp. nov. isolated from humans and animals with diarrheal illness. J Clin Microbiol 29:376–385. https://doi.org/10.1128/jcm.29.2.376-385.1991
41. Ward B. 2015. Bacterial energy metabolism, p 201–233. In Molecular medical microbiology
42. Perez JC, Groisman EA. 2009. Evolution of transcriptional regulatory circuits in bacteria. Cell 138:233–244. https://doi.org/10.1016/j.cell.2009.07.002
43. Federowicz S, Kim D, Ebrahim A, Lerman J, Nagarajan H, Cho B, Zengler K, Palsson B. 2014. Determining the control circuitry of redox metabolism at the genome-scale. PLoS Genet 10:e1004264. https://doi.org/10.1371/journal.pgen.1004264

44. Myers KS, Yan H, Ong IM, Chung D, Liang K, Tran F, Keleş S, Landick R, Kiley PJ. 2013. Genome-scale analysis of *Escherichia coli* FNR reveals complex features of transcription factor binding. PLoS Genet 9:e1003565. https://doi.org/10.1371/journal.pgen.1003565
45. Brown AN, Anderson MT, Bachman MA, Mobley HLT. 2022. The ArcAB two-component system: function in metabolism, redox control, and infection. Microbiol Mol Biol Rev 86:e0011021. https://doi.org/10.1128/mmbr.00110-21
46. Park DM, Akhtar MS, Ansari AZ, Landick R, Kiley PJ. 2013. The bacterial response regulator ArcA uses a diverse binding site architecture to regulate carbon oxidation globally. PLoS Genet 9:e1003839. https://doi.org/10.1371/journal.pgen.1003839
47. Stewart V. 1994. Dual interacting two-component regulatory systems mediate nitrate- and nitrite-regulated gene expression in *Escherichia coli*. Res Microbiol 145:450–454. https://doi.org/10.1016/0923-2508(94)90093-0
48. Iyer MS, Pal A, Srinivasan S, Somvanshi PR, Venkatesh KV. 2021. Global transcriptional regulators fine-tune the translational and metabolic efficiency for optimal growth of *Escherichia coli*. mSystems 6:e00001-21. https://doi.org/10.1128/mSystems.00001-21
49. Overton TW, Griffiths L, Patel MD, Hobman JL, Penn CW, Cole JA, Constantinidou C. 2006. Microarray analysis of gene regulation by oxygen, nitrate, nitrite, FNR, NarL and NarP during anaerobic growth of *Escherichia coli*: new insights into microbial physiology. Biochem Soc Trans 34:104–107. https://doi.org/10.1042/BST0340104
50. Unden G, Bongaerts J. 1997. Alternative respiratory pathways of *Escherichia coli*: energetics and transcriptional regulation in response to electron acceptors. Biochim Biophys Acta 1320:217–234. https://doi.org/10.1016/s0005-2728(97)00034-0
51. van der Stel A-X, van Mourik A, Heijmen-van Dijk L, Parker CT, Kelly DJ, van de Lest CHA, van Putten JPM, Wösten MMSM. 2015. The *Campylobacter jejuni* RacRS system regulates fumarate utilization in a low oxygen environment. Environ Microbiol 17:1049–1064. https://doi.org/10.1111/1462-2920.12476
52. Liu X, Gao B, Novik V, Galán JE. 2012. Quantitative proteomics of intracellular *Campylobacter jejuni* reveals metabolic reprogramming. PLoS Pathog 8:e1002562. https://doi.org/10.1371/journal.ppat.1002562
53. Bell TH, Bell T. 2020. Many roads to bacterial generalism. FEMS Microbiol Ecol 97:240. https://doi.org/10.1093/femsec/fiaa240
54. Bury-Moné S, Kaakoush NO, Asencio C, Mégraud F, Thibonnier M, De Reuse H, Mendz GL. 2006. Is *Helicobacter pylori* a true microaerophile? Helicobacter 11:296–303. https://doi.org/10.1111/j.1523-5378.2006.00413.x
55. Pelliciari S, Pinatel E, Vannini A, Peano C, Puccio S, De Bellis G, Danielli A, Scarlato V, Roncarati D. 2017. Insight into the essential role of the *Helicobacter pylori* HP1043 orphan response regulator: genome-wide identification and characterization of the DNA-binding sites. Sci Rep 7:41063. https://doi.org/10.1038/srep41063
56. Olekhnovich IN, Vitko S, Valliere M, Hoffman PS. 2014. Response to metronidazole and oxidative stress is mediated through homeostatic regulator HsrA (HP1043) in *Helicobacter pylori*. J Bacteriol 196:729–739. https://doi.org/10.1128/JB.01047-13
57. Loh JT, Shum MV, Jossart SDR, Campbell AM, Sawhney N, McDonald WH, Scholz MB, McClain MS, Forsyth MH, Cover TL. 2021. Delineation of the pH-responsive regulon controlled by the *Helicobacter pylori* ArsRS two-component system. Infect Immun 89:e00597-20. https://doi.org/10.1128/IAI.00597-20
58. Vannini A, Pinatel E, Costantini PE, Pelliciari S, Roncarati D, Puccio S, De Bellis G, Peano C, Danielli A. 2017. Comprehensive mapping of the *Helicobacter pylori* NikR regulon provides new insights in bacterial nickel responses. Sci Rep 7:45458. https://doi.org/10.1038/srep45458
59. Gölz G, Kittler S, Malakauskas M, Alter T. 2018. Survival of *Campylobacter* in the food chain and the environment. Curr Clin Micro Rpt 5:126–134. https://doi.org/10.1007/s40588-018-0092-z
60. Dufour V, Li J, Flint A, Rosenfeld E, Rivoal K, Georgeault S, Alazzam B, Ermel G, Stintzi A, Bonnaure-Mallet M, Baysse C. 2013. Inactivation of the LysR regulator Cj1000 of *Campylobacter jejuni* affects host colonization and respiration. Microbiology (Reading) 159:1165–1178. https://doi.org/10.1099/mic.0.062992-0
61. Svensson SL, Huynh S, Parker CT, Gaynor EC. 2015. The *Campylobacter jejuni* CprRS two-component regulatory system regulates aspects of the cell envelope. Mol Microbiol 96:189–209. https://doi.org/10.1111/mmi.12927
62. Fields JA, Li J, Gulbronson CJ, Hendrixson DR, Thompson SA. 2016. *Campylobacter jejuni* CSRA regulates metabolic and virulence associated proteins and is necessary for mouse colonization. PLoS One 11:e0156932. https://doi.org/10.1371/journal.pone.0156932
63. Price EE, Román-Rodríguez F, Boyd JM. 2021. Bacterial approaches to sensing and responding to respiration and respiration metabolites. Mol Microbiol 116:1009–1021. https://doi.org/10.1111/mmi.14795
64. Contreras M, Thiberge JM, Mandrand-Berthelot MA, Labigne A. 2003. Characterization of the roles of NikR, a nickel-responsive pleiotropic autoregulator of *Helicobacter pylori*. Mol Microbiol 49:947–963. https://doi.org/10.1046/j.1365-2958.2003.03621.x
65. Atabay HI, Corry JEL. 1998. Evaluation of a new *Arcobacter* enrichment medium and comparison with two media developed for enrichment of *Campylobacter* spp. Int J Food Microbiol 41:53–58. https://doi.org/10.1016/s0168-1605(98)00034-8
66. Beauchamp JM, Leveque RM, Dawid S, DiRita VJ. 2017. Methylation-dependent DNA discrimination in natural transformation of *Campylobacter jejuni*. Proc Natl Acad Sci U S A 114:E8053–E8061. https://doi.org/10.1073/pnas.1703331114
67. Gibson DG, Young L, Chuang RY, Venter JC, Hutchison CA, Smith HO. 2009. Enzymatic assembly of DNA molecules up to several hundred kilobases. Nat Methods 6:343–345. https://doi.org/10.1038/nmeth.1318
68. Dalia AB, McDonough E, Camilli A. 2014. Multiplex genome editing by natural transformation. Proc Natl Acad Sci U S A 111:8937–8942. https://doi.org/10.1073/pnas.1406478111
69. Cieślak M. 2021. Construction of the plasmid for the analysis of the essentiality of the Abu0127 gene for the survival of *Arcobacter butzleri* RM4018. Wroclaw University of Science and Technology.
70. Perkins A, Tudorica DA, Amieva MR, Remington SJ, Guillemin K. 2019. *Helicobacter pylori* senses bleach (HOCl) as a chemoattractant using a cytosolic chemoreceptor. PLoS Biol 17:e3000395. https://doi.org/10.1371/journal.pbio.3000395
71. Langmead B, Salzberg SL. 2012. Fast gapped-read alignment with Bowtie 2. Nat Methods 9:357–359. https://doi.org/10.1038/nmeth.1923
72. Langmead B, Wilks C, Antonescu V, Charles R. 2019. Scaling read aligners to hundreds of threads on general-purpose processors. Bioinformatics 35:421–432. https://doi.org/10.1093/bioinformatics/bty648
73. Li H, Handsaker B, Wysoker A, Fennell T, Ruan J, Homer N, Marth G, Abecasis G, Durbin R, 1000 Genome Project Data Processing Subgroup. 2009. The sequence alignment/map format and SAMtools. Bioinformatics 25:2078–2079. https://doi.org/10.1093/bioinformatics/btp352
74. Liao Y, Smyth GK, Shi W. 2019. The R package Rsubread is easier, faster, cheaper and better for alignment and quantification of RNA sequencing reads. Nucleic Acids Res 47:e47. https://doi.org/10.1093/nar/gkz114
75. Robinson MD, McCarthy DJ, Smyth GK. 2010. edgeR: a bioconductor package for differential expression analysis of digital gene expression data. Bioinformatics 26:139–140. https://doi.org/10.1093/bioinformatics/btp616
76. Chen Y, Lun ATL, Smyth GK. 2016. From reads to genes to pathways: differential expression analysis of RNA-seq experiments using Rsubread and the edgeR quasi-likelihood pipeline. F1000Res 5:1438. https://doi.org/10.12688/f1000research.8987.1
77. Blighe K, Rana S, Lewis M. EnhancedVolcano: publication-ready volcano plots with enhanced colouring and labeling. Available from: https://bioconductor.org/packages/devel/bioc/vignettes/EnhancedVolcano/inst/doc/EnhancedVolcano.html. Retrieved 21 Aug 2022.
78. Abele M, Doll E, Bayer FP, Meng C, Lomp N, Neuhaus K, Scherer S, Kuster B, Ludwig C. 2023. Unified workflow for the rapid and in-depth characterization of bacterial proteomes. Mol Cell Proteomics 22:100612. https://doi.org/10.1016/j.mcpro.2023.100612
79. Doellinger J, Schneider A, Hoeller M, Lasch P. 2020. Sample preparation by easy extraction and digestion (SPEED) - a universal, rapid, and detergent-free protocol for proteomics based on acid extraction. Mol Cell Proteomics 19:209–222. https://doi.org/10.1074/mcp.TIR119.001616
80. Cox J, Neuhauser N, Michalski A, Scheltema RA, Olsen JV, Mann M. 2011. Andromeda: a peptide search engine integrated into the maxquant environment. J Proteome Res 10:1794–1805. https://doi.org/10.1021/pr101065j

81. Tyanova S, Temu T, Cox J. 2016. The MaxQuant computational platform for mass spectrometry-based shotgun proteomics. Nat Protoc 11:2301–2319. https://doi.org/10.1038/nprot.2016.136
82. Cox J, Hein MY, Luber CA, Paron I, Nagaraj N, Mann M. 2014. Accurate proteome-wide label-free quantification by delayed normalization and maximal peptide ratio extraction, termed MaxLFQ. Mol Cell Proteomics 13:2513–2526. https://doi.org/10.1074/mcp.M113.031591
83. Benjamini Y, Hochberg Y. 1995. Controlling the false discovery rate: a practical and powerful approach to multiple testing. J R Stat Soc B 57:289–300. https://doi.org/10.1111/j.2517-6161.1995.tb02031.x
84. GitHub - mengchen18/omicsViewer. Available from: https://github.com/mengchen18/omicsViewer. Retrieved 23 Jan 2024.
85. Kanehisa M, Furumichi M, Tanabe M, Sato Y, Morishima K. 2017. KEGG: new perspectives on genomes, pathways, diseases and drugs. Nucleic Acids Res 45:D353–D361. https://doi.org/10.1093/nar/gkw1092
86. Huerta-Cepas J, Szklarczyk D, Heller D, Hernández-Plaza A, Forslund SK, Cook H, Mende DR, Letunic I, Rattei T, Jensen LJ, von Mering C, Bork P. 2019. eggNOG 5.0: a hierarchical, functionally and phylogenetically annotated orthology resource based on 5090 organisms and 2502 viruses. Nucleic Acids Res 47:D309–D314. https://doi.org/10.1093/nar/gky1085
87. Galperin MY, Makarova KS, Wolf YI, Koonin EV. 2015. Expanded microbial genome coverage and improved protein family annotation in the COG database. Nucleic Acids Res 43:D261–D269. https://doi.org/10.1093/nar/gku1223
88. Perez-Riverol Y, Bai J, Bandla C, García-Seisdedos D, Hewapathirana S, Kamatchinathan S, Kundu DJ, Prakash A, Frericks-Zipper A, Eisenacher M, Walzer M, Wang S, Brazma A, Vizcaíno JA. 2022. The PRIDE database resources in 2022: a hub for mass spectrometry-based proteomics evidences. Nucleic Acids Res 50:D543–D552. https://doi.org/10.1093/nar/gkab1038

Supplemental Material

CemR atypical response regulator impacts energy conversion in *Campylobacteria*

This PDF file includes:

Supplementary Tables

Tab. S1: Strains, plasmids and proteins used in this study.

Tab. S2: Primers used in this study.

Supplementary Figures

Fig. S1: Disc diffusion assay of *C. jejuni* and *A. butzleri* indicating the influence of Cj1608 and Abu0127 on resistance to oxidative agents.

Fig. S2: RNA-seq analysis of *C. jejuni* gene transcription controlled by Cj1608.

Fig. S3: RNA-seq analysis of *A. buzleri* gene transcription controlled by Abu0127.

Fig. S4: LC-MS/MS analysis of *C. jejuni* and *A. butzleri* protein level regulation mediated by Cj1608 and Abu0127, respectively.

Fig. S5: Pearson correlation analysis between proteomics and transcriptomics data of *C. jejuni* and *A. butzleri*.

Fig. S6: The KEGG pathway enrichment of *C. jejuni* citrate cycle.

Fig. S7: The KEGG pathway enrichment of *A. butzleri* oxidative phosphorylation and citrate cycle.

Fig. S8: Transcriptomics and proteomics data of citrate synthetase operon.

Fig. S9: Transcriptomics and proteomics data of NADH-quinone oxidoreductase operon.

Fig. S10: Impact of HP1021 on gene regulation in *H. pylori*.

Fig. S11: *C. jejuni* NCTC 11168 ΔCj1608 knock-out mutant construction.

Fig. S12: *A. butzleri* RM4018 ΔAbu0127 knock-out mutant construction

Fig. S13: The reproducibility of *C. jejuni* and *A. butzleri* biological replicates in omics data.

Description of Additional Supplemental Materials

Supplemental Material References

Table S1: Strains, plasmids and proteins used in this study.

Strain	Relevant features	Reference/source
E. coli DH5α	*supE44*, *hsdR17*, *recA1*, *endA1*, *gyrA1*, *gyrA96*, *thi-1*, *relA1*	(1)
E. coli BL21	F-, *ompT*, *hsdS (rB-*, *mB-)*, *gal*, *dcm*	GE Healthcare
C. jejuni NCTC 11168	Parental strain	(2)
C. jejuni NCTC 11168 ΔCj1608	Δ*Cj1608*::*aphA-3*; 11168 with *Cj1608* exchanged to *aphA-3* cassette	This study
C. jejuni NCTC 11168 C_{Cj1608}	(Δ*Cj1608*::*aphA-3*)::*Cj1608*, *hdsM*::*cat*; 11168 ΔCj1608 in which *aphA-3* was exchanged to *Cj1608* and *cat* cassette was inserted in to *hsdM* gene	This study
A. butzleri RM4018	Parental strain	(3), DSMZ-German Collection of Microorganisms and Cell Cultures GmbH
A. butzleri RM4018 ΔAbu0127	Δ*Abu0127*::*aphA-3*; Abu0127 exchanged to *aphA-3* cassette	This study

Plasmid	Relevant features	Reference/source
pUC18	Cloning vector, Amp^R	Thermo Fisher Scientific
pCR2.1-TOPO®	TA cloning vector, Amp^R, Kan^R	Thermo Fisher Scientific
pCR2.1/ΔCj1608	pUC18 derivative containing *Cj1608* flanking regions and *aphA-3* for allelic exchange of *Cj1608* for *aphA-3*	This study
pTZ57R/TΔHP1021	pTZ57R/T derivative containing *aphA-3* gene	(4)
pUC18/COM/Cj1608	pUC18 derivative containing *Cj1608* flanking regions and *Cj1608* for allelic exchange of *aphA-3* for *Cj1608*	This study
pSB3021	Suicide vector for integration of *cat* gene in *hsdM* gene for complementation	(5)
pUC18/ΔAbu0127	pUC18 derivative containing *Abu0127* flanking regions and *aphA-3* for allelic exchange of *Abu0127* for *aphA-3*	(6)
pET28/StrepCj1608	pET28Strep derivative containing the *Cj1608* gene for protein expression	This study
pET28/StrepAbu0127	pET28Strep derivative containing the *Abu0127* gene for protein expression	This study

Recombinant protein	Relevant features	Reference/source
StrepCj1608	Recombinant, *C. jejuni* Cj1608 protein, Strep-tagged at N-terminus, purified from *E. coli*	This study
StrepAbu0127	Recombinant, *A. butzleri* Abu0127 protein, Strep-tagged at N-terminus, purified from *E. coli*	This study

Table S2: Primers used in this study.

Oligo name	Sequence (5' → 3')
P1	gatcaaaacctagaatttacagatg
P2	cacccgggtaccgagtcataatcttgtccaatcaaaatatt
P3	tggacaagattatgactcggtacccgggtgactaa
P4	ctgatttcatatttcttcctttctaaaacaattcatccagtaaaatatag
P5	ctatattttactggatgaattgttttagaaaggaagaaatatgaaatcag
P6	ctgctttatcaatagtccaacg
P7	cagatacaacacttttgacaatg
P8	gctcgacatactgttcttccc
P9	acagctatatccagcatcacttag
P10	gtcgactctagaggatccccggatttaaagcacatagtgatgg
P11	ctcctagttagtcaggatcctcatctttttttccaattataatat
P12	ggatcctgactaactaggaggaataaatg
P13	ctaaaacaattcatccagtaaaat
P14	ttttactggatgaattgttttaggggataatgtatgaatttgagaaa
P15	cgaattcgagctcggtacccccctgcaataatatcatcaccc
P16	ttttgacattcatgcctttgaagag
P17	gataaaccgcagctgttgcaatt
P18	gtttgttttcagcaagccactc
P19	gccaagcgttgtagatatgtca
P23	aaaccaccagaacaggcaca
P24	tgacgtttcaagatttggagcag
P25	taccataacccatagcaccgat
P26	agaaattgaaggcgatatgggc
P27	tctggaccttgaacaaattgca
P28	agccttcggttcttcctaca
P29	cgggatccatgaaagttttaattattgaaaatg
P30	ccggtcgacttatttttcttgctgatttcata
P31	cgggatccatgaacatattaattatcgaaaatg
P32	ccggtcgacctatttctttttttcgatatctag
P33	ggagtaagaatagcttcgaatggcccagttgtaccgtcatata
P34	ctttattcagcgcttattttaacagc
P35	ggagtaagaatagcttcgaatgaatagctgctcttgaagcagc
P36	cgctatcaaataccatgcgac
P37	ggagtaagaatagcttcgaatcaatgaaaattgtggaagct
P38	agattgaatacagctttgagt
P39	ggagtaagaatagcttcgaattccacttgttataagttcatcattt
P40	acttgatattagaagaattgcaact
P41	FAM-ggagtaagaatagcttcgaat*
P42	Cy5- ggagtaagaatagcttcgaat**
P43	cggaatttgacattttcgctcc
P44	gcggttatttgaggctattattgttatga
P45	gtggaagctaatattaattccgttgaca
P46	tgtttcttttggtagcaacgga

* - FAM, 6-fluorescein amidite;

** - Cy5, tetramethylindo(di)-carbocyanines 5.

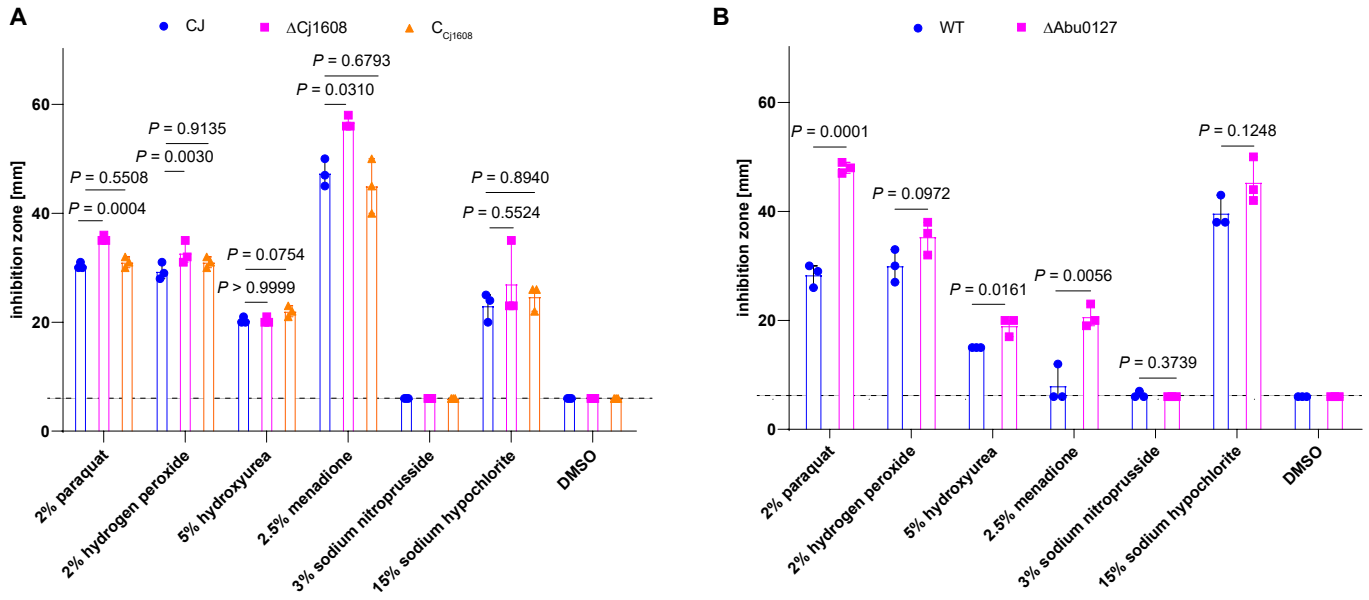

S1 Fig. Disc diffusion assay of *C. jejuni* and *A. butzleri* indicating the influence of Cj1608 and Abu0127 on resistance to oxidative agents. (A) *C. jejuni* wild-type (CJ)), Cj1608 knock-out mutant (ΔCj1608) and Cj1608 complementation (C_{Cj1608}), and **(B)** *A. butzleri* wild-type (AB) and Abu0127 knock-out mutant (ΔAbu0127) strains were analyzed. The black dashed lines indicate the disc size. Data have been depicted as the mean values ± SD. n = 3 biologically independent experiments. **(A)** Ordinary one-way ANOVA with Tukey's multiple comparison test determined the P value. **(B)** The students' paired t-test determined the P value. Data taken from (6).

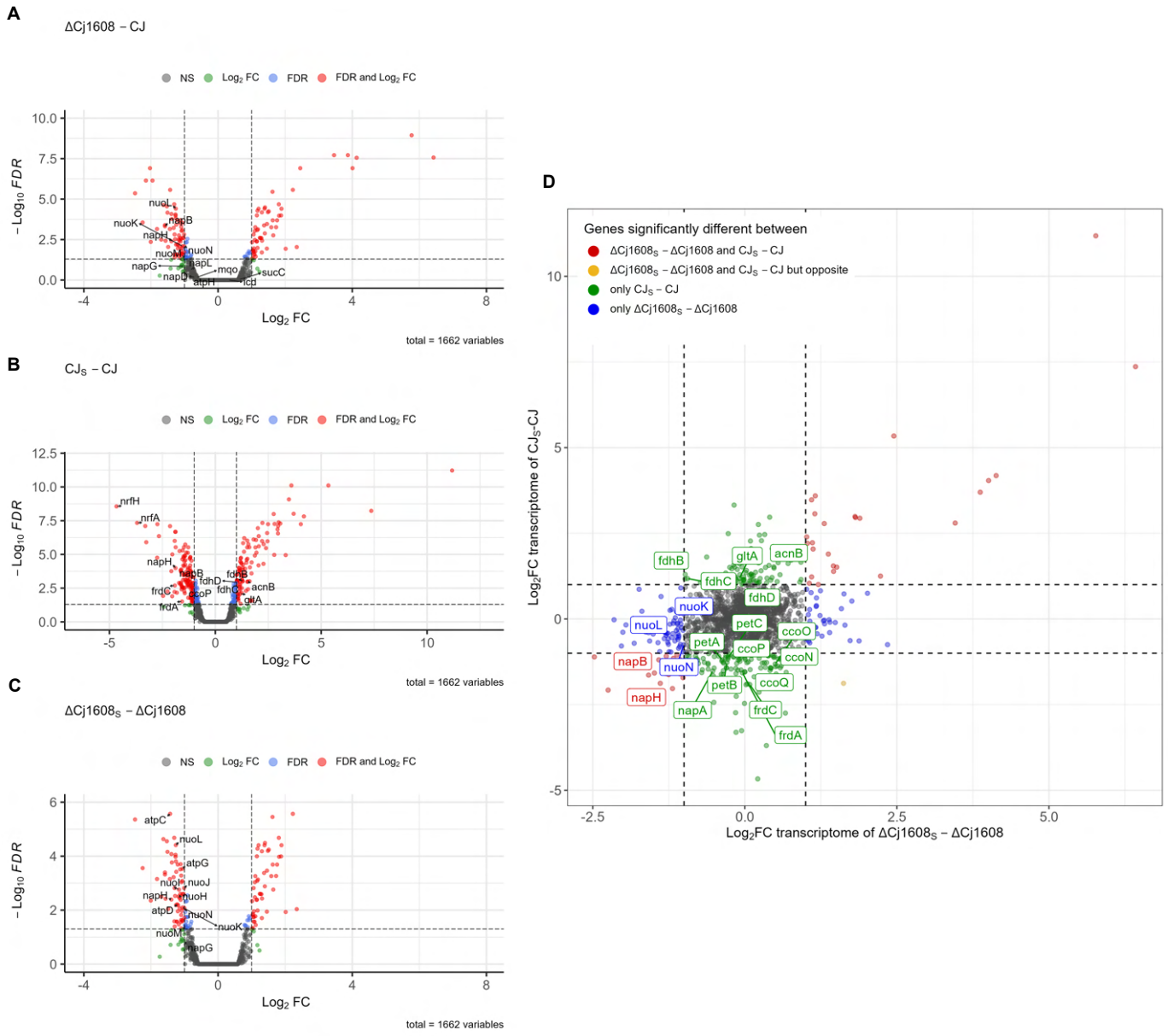

S2 Fig. RNA-seq analysis of *C. jejuni* gene transcription controlled by Cj1608. (A) The Volcano plot of genes differently transcribed in the Cj1608 knock-out mutant (ΔCj1608) strain compared to the *C. jejuni* wild-type (CJ) strain (ΔCj1608-CJ). **(B)** The Volcano plot of genes differently transcribed in the CJ strain under oxidative stress induced by 1 mM paraquat (CJ_S) compared to the non-stressed wild-type strain (CJ_S-CJ). **(C)** Volcano plot of genes differently transcribed in the ΔCj1608 strain under oxidative stress induced by 1 mM paraquat ($\Delta Cj1608_S$) compared to the non-stressed ΔCj1608 mutant ($\Delta Cj1608_S$-ΔCj1608). **(D)** The comparison of gene transcription in the *C. jejuni* CJ, CJ_S, ΔCj1608 and stressed $\Delta Cj1608_S$ cells revealed by RNA-seq. The genes signed on the graph correspond to the citric acid cycle and electron transport chain. **(A-D)** Values outside the black dashed lines indicate a change in the expression of $|\log_2 FC| \geq 1$. Grey dots correspond to genes whose transcription was not significantly changed (FDR ≤ 0.05). Genes whose transcription significantly changed ($|\log_2 FC| \geq 1$; FDR ≤ 0.05) are depicted by colored dots; see the legend in the figure.

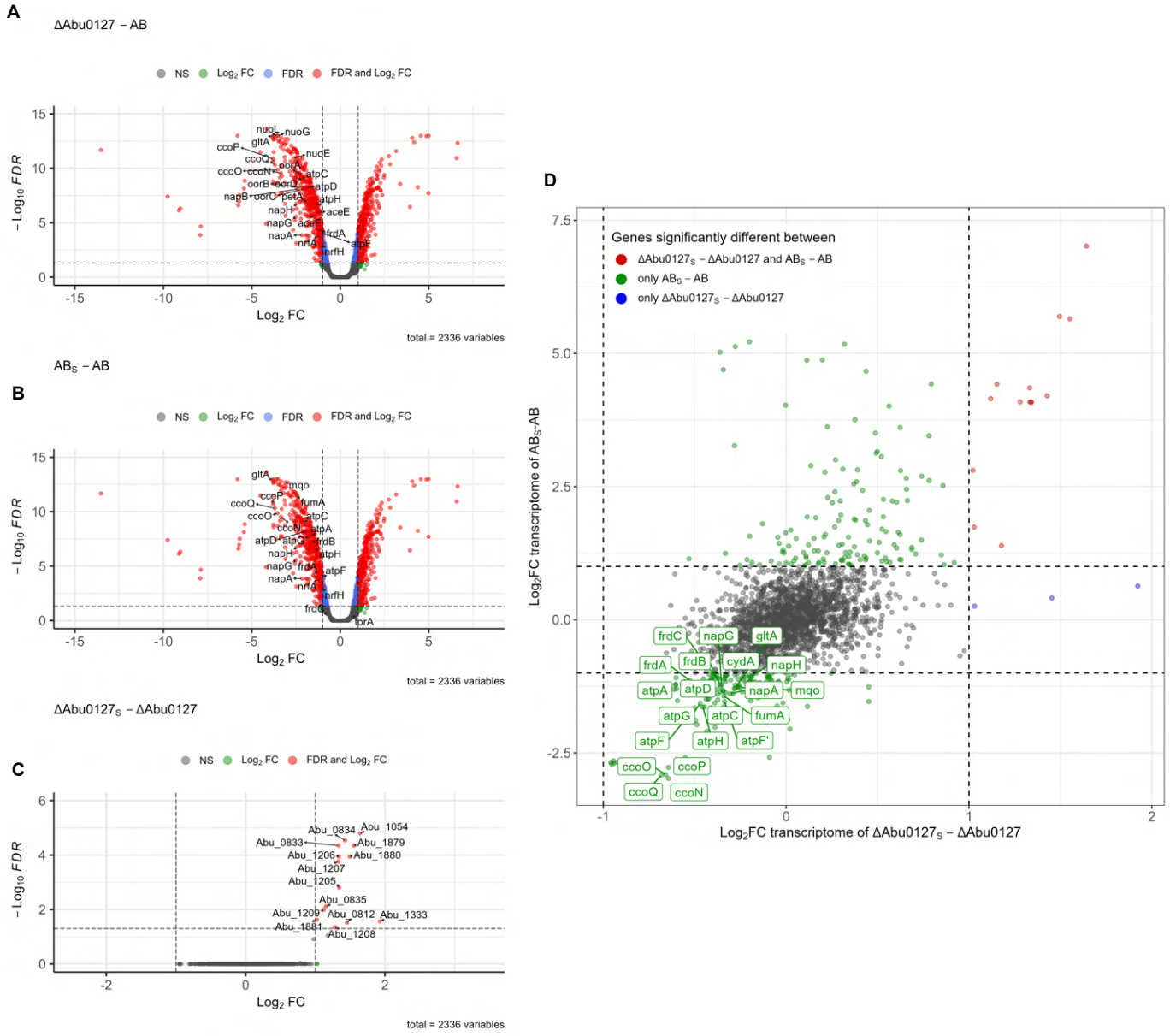

S3 Fig. RNA-seq analysis of *A. butzleri* gene transcription controlled by Abu0127. (A) The Volcano plot of genes differently transcribed in the Abu0127 knock-out mutant (ΔAbu0127) strain compared to the *A. butzleri* wild-type (AB) strain(ΔAbu0127-AB). **(B)** The Volcano plot of genes differently transcribed in the AB strain under oxidative stress induced by 1 mM paraquat (AB_S) compared to the non-stressed wild-type strain (AB_S-AB). **(C)** Volcano plot of genes differently transcribed in the ΔAbu0127 strain under oxidative stress induced by 1 mM paraquat ($\Delta Abu0127_S$) compared to the non-stressed ΔAbu0127 mutant ($\Delta Abu0127_S$-ΔAbu0127). **(D)** The comparison of gene transcription in the *A. butzleri* AB, AB_S, ΔAbu0127 and stressed $\Delta Abu0127_S$ cells revealed by RNA-seq. The genes signed on the graph correspond to the citric acid cycle and electron transport chain. **(A-D)** Values outside the black dashed lines indicate a change in the expression of $|\log_2 FC| \geq 1$. Grey dots correspond to genes whose transcription was not significantly changed (FDR ≤ 0.05). Genes whose transcription significantly changed ($|\log_2 FC| \geq 1$; FDR ≤ 0.05) are depicted by colored dots; see the legend in the figure.

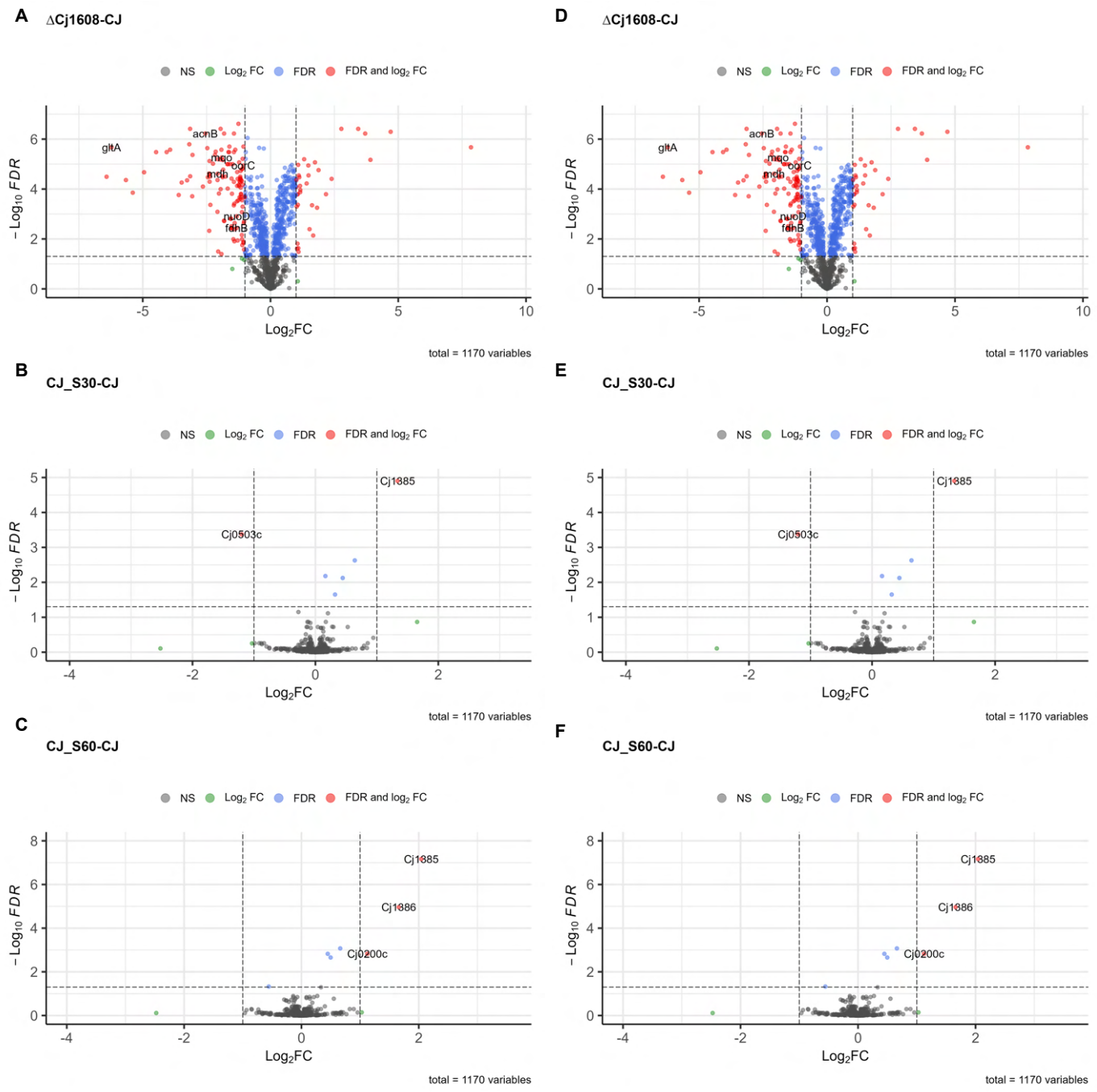

S4 Fig. LC-MS/MS analysis of *C. jejuni* and *A. butzleri* protein level regulation mediated by Cj1608 and Abu0127, respectively. (A) Volcano plot of proteins differently expressed in the Cj1608 knock-out mutant (ΔCj1608) strain compared to the *C. jejuni* wild-type (CJ) strain (ΔCj1608-CJ). **(B)** Volcano plot of proteins differentially expressed in the CJ strain after 30-min oxidative stress (CJ_S30) induced by 1 mM paraquat compared to the non-stressed wild-type strain (CJ_S30-CJ). **(C)** Volcano plot of proteins differentially expressed in the CJ strain after 60 min of oxidative stress (CJ_S60) induced by 1 mM paraquat compared to the non-stressed CJ strain (CJ_S60-CJ). **(D)** Volcano plot of proteins differently expressed in the Abu0127 knock-out mutant (ΔAbu0127)strain compared to the *A. butzleri* wild-type (AB) strain (ΔAbu0127-AB). **(E)** Volcano plot of proteins differentially expressed in the AB strain after 30-min oxidative stress (AB_S30) induced by 1 mM paraquat compared to the non-stressed AB strain (AB_S30-AB). **(F)** Volcano plot of proteins differentially expressed in the AB strain after 60 min of oxidative stress (AB_S60) induced by 1 mM paraquat compared to the non-stressed AB strain (AB_S60-AB). **(A-F)** n = 4 biologically independent experiments. Green dots correspond to genes with $|\log_2 FC| \geq 1$ and FDR ≥ 0.05; blue dots correspond to genes with $|\log_2 FC| \leq 1$ and FDR ≤ 0.05; red dots correspond to genes with $|\log_2 FC| \geq 1$ and FDR ≤ 0.05; grey dots correspond to genes that were not significantly changed. NS, non-significant. FDR, false discovery rate.

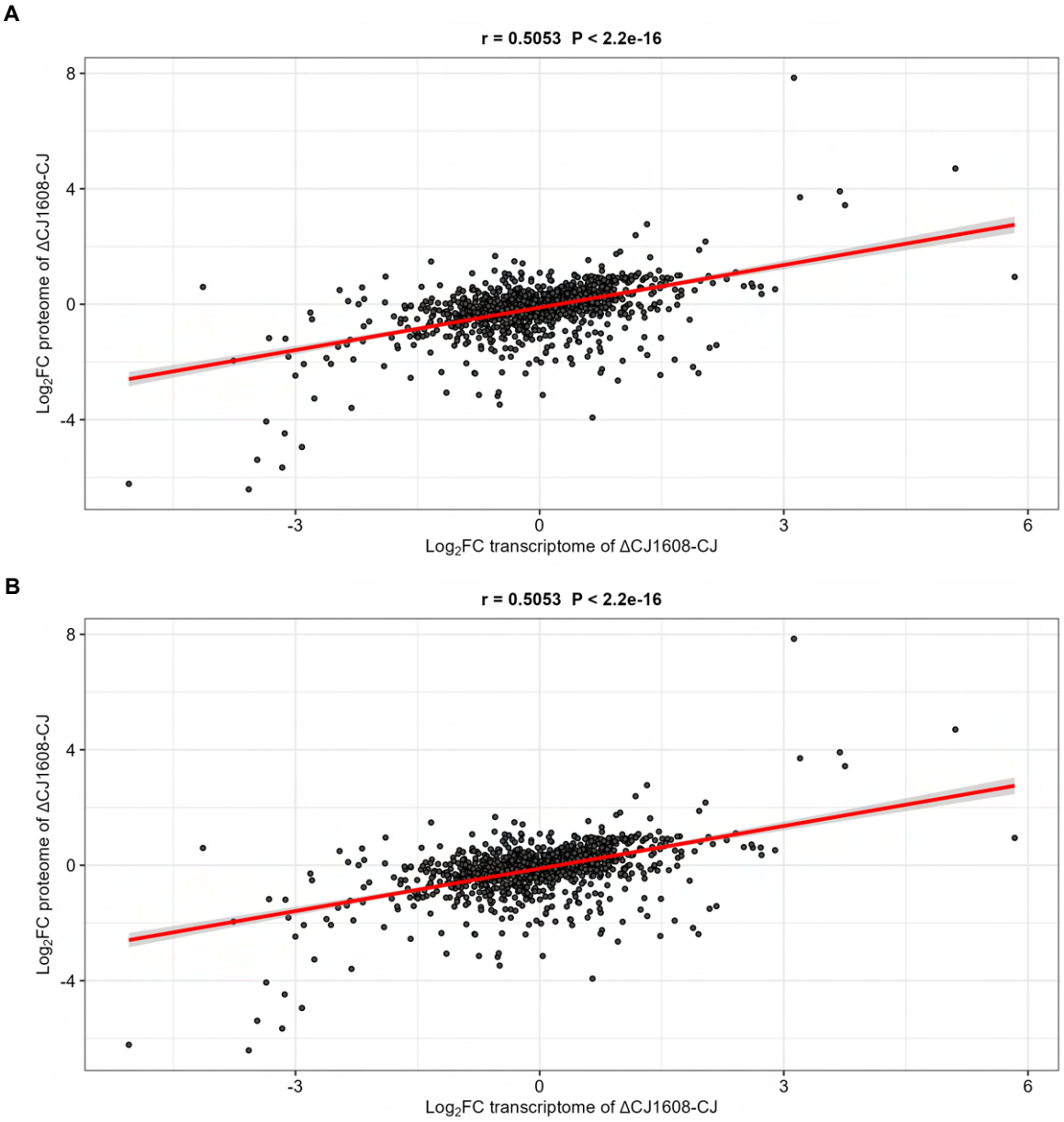

S5 Fig. Pearson correlation analysis between proteomics and transcriptomics data of (A) *C. jejuni* and **(B)** *A. butzleri*. Scatter plots of the correlation between data sets of the $\log_2$FC of gene transcript (x-axis) and proteome (y-axis) of ΔCj1608-CJ and ΔAbu0127-AB, respectively. The red line represents the regression line; r, Pearson correlation coefficient.

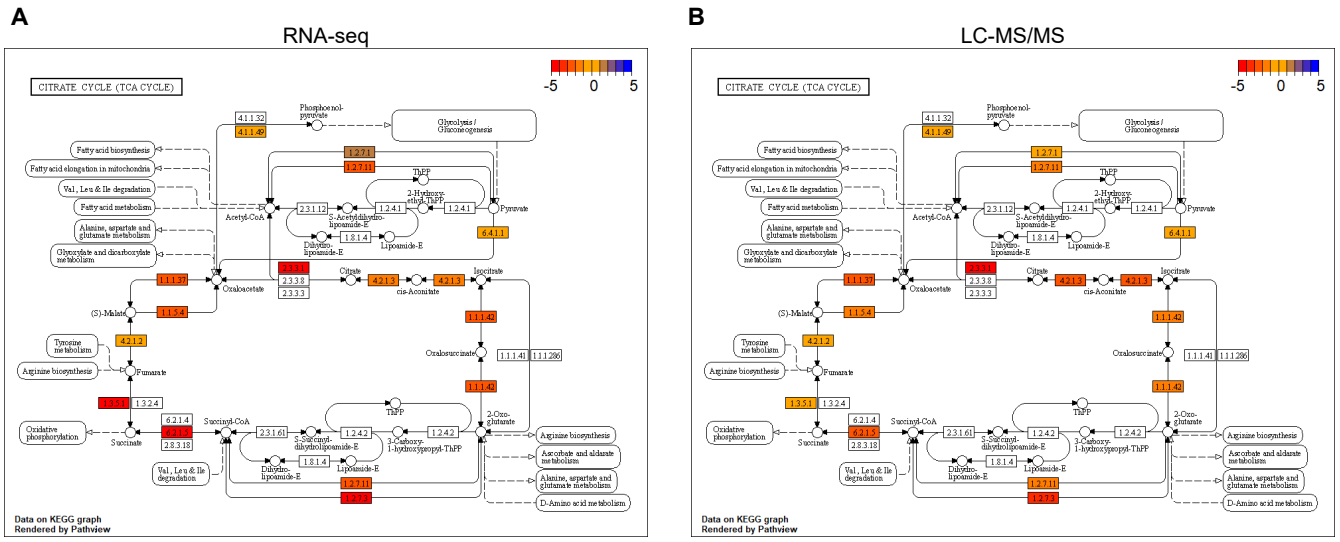

S6 Fig. The KEGG pathway enrichment of *C. jejuni* citrate cycle. (A) Gene enrichment of the citrate cycle KEGG group visualized by ClusterProfiler. Gene expression values are mapped to a gradient color scale of $\log_2$FC. **(B)** Protein enrichment of the citrate cycle KEGG group visualised by ClusterProfiler. Protein expression values are mapped to a gradient color scale of $\log_2$FC.

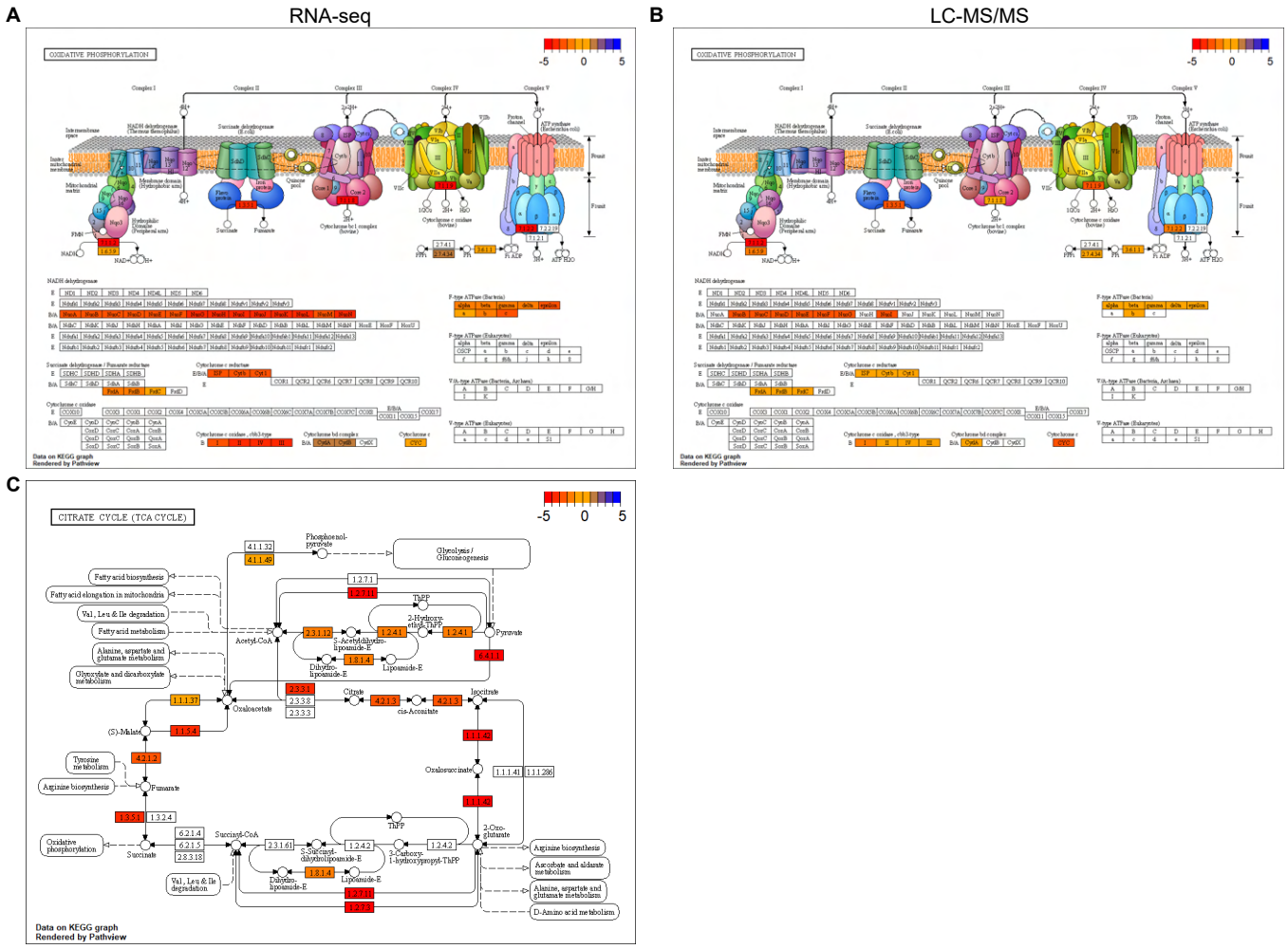

S7 Fig. The KEGG pathway enrichment of *A. butzleri* oxidative phosphorylation and citrate cycle. (A) Gene enrichment of oxidative phosphorylation KEGG group visualized by ClusterProfiler. Gene expression values are mapped to a gradient colour scale of $\log_2$FC. **(B)** Protein enrichment of oxidative phosphorylation KEGG group visualized by ClusterProfiler. Protein expression values are mapped to a gradient colour scale of $\log_2$FC. **(C)** Gene enrichment of the citrate cycle KEGG group visualized by ClusterProfiler. Protein expression values are mapped to a gradient color scale of $\log_2$FC.

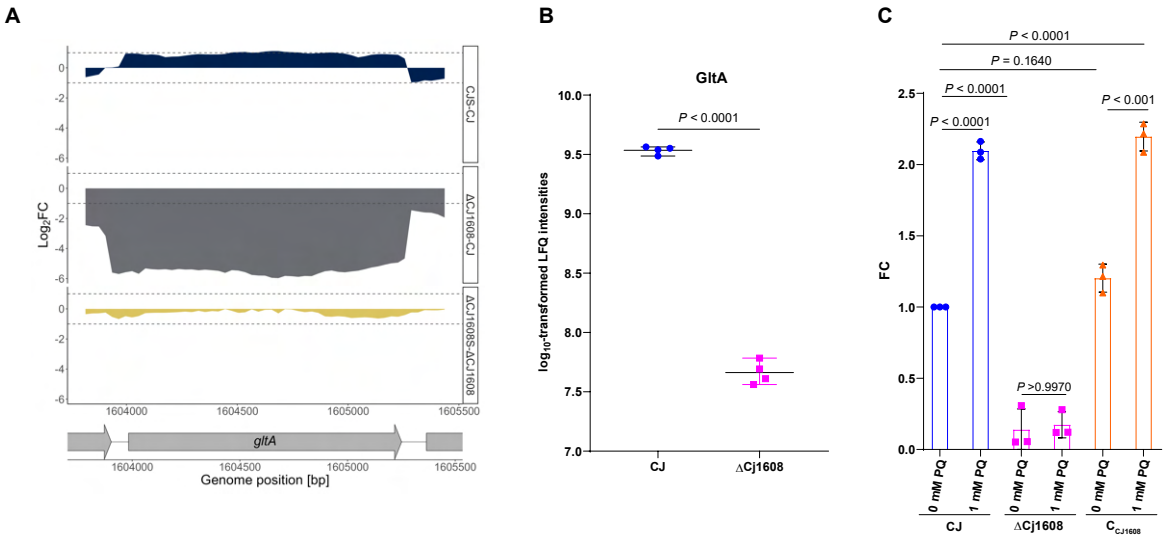

S8 Fig. Transcriptomics and proteomics data of citrate synthetase operon. (A) RNA-seq data profile comparing *gltA* transcription in *C. jejuni* wild-type (CJ), Cj1608 knock-out mutant (ΔCj1608) strains under microaerobic growth and paraquat-induced oxidative stress. Values above the black dashed lines indicate a change in the expression of $|\log_2 FC| \geq 1$; FDR ≤ 0.05. **(B)** Logarithmically transformed LFQ intensities of GltA protein in CJ and ΔCj1608 strains. The student's unpaired t-test determined the P value. n = 4 biologically independent experiments. **(C)** RT-qPCR analysis of *gltA* transcription in CJ, ΔCj1608 and Cj1608 complementation (C_{Cj1608}) strains cells cultured under microaerobic or paraquat-induced oxidative stress conditions. n = 3 biologically independent experiments. Data presented as the mean values ± SD. Ordinary one-way ANOVA with Tukey's multiple comparison test determined the P value.

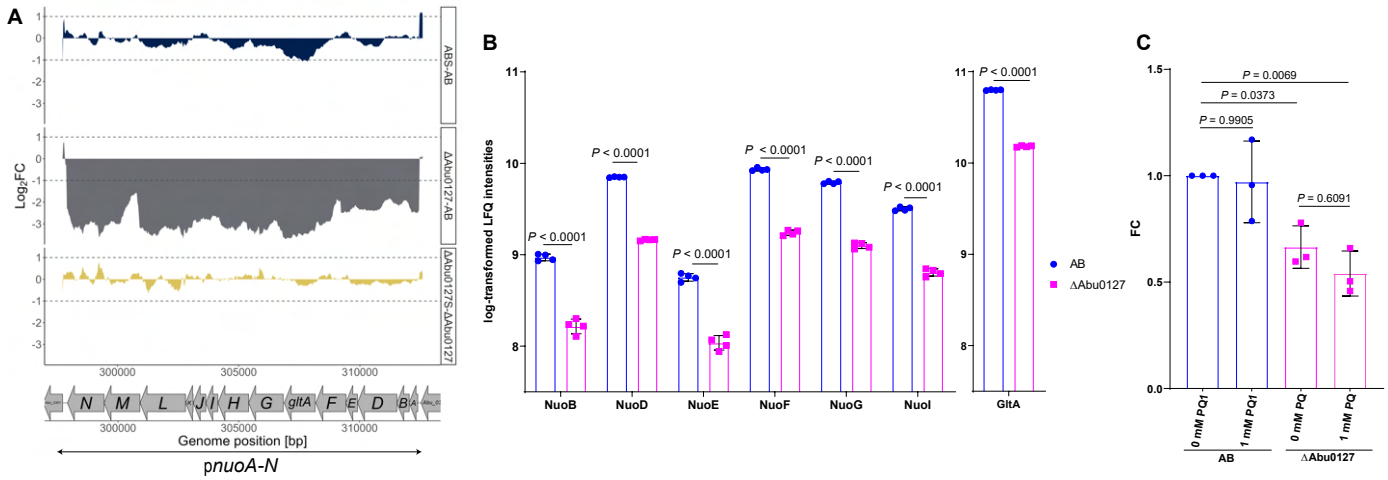

S9 Fig. Transcriptomics and proteomics data of NADH-quinone oxidoreductase operon. (A) RNA-seq data profile comparing the transcription of the *nuo* operon in *A. butzleri* wild-type (AB) and Abu0127 knock-out mutant (ΔAbu0127) strains under microaerobic growth and paraquat-induced oxidative stress Values above the black dashed lines indicate a change in the expression of $|\log_2 FC| \geq 1$; FDR ≤ 0.05. **(B)** Logarithmically transformed LFQ intensities of Nuo B-F, GltA, NuoG, and NuoI proteins in AB and ΔAbu0127 strains. n = 4 biologically independent experiments. **(C)** RT-qPCR analysis of *nuoB* transcription in AB and ΔAbu0127 cells cultured under microaerobic or paraquat-induced oxidative stress conditions. **(B and C)** Data presented as the mean values ± SD. Ordinary one-way ANOVA with Tukey's multiple comparison test determined the P value. n = 3 biologically independent experiments.

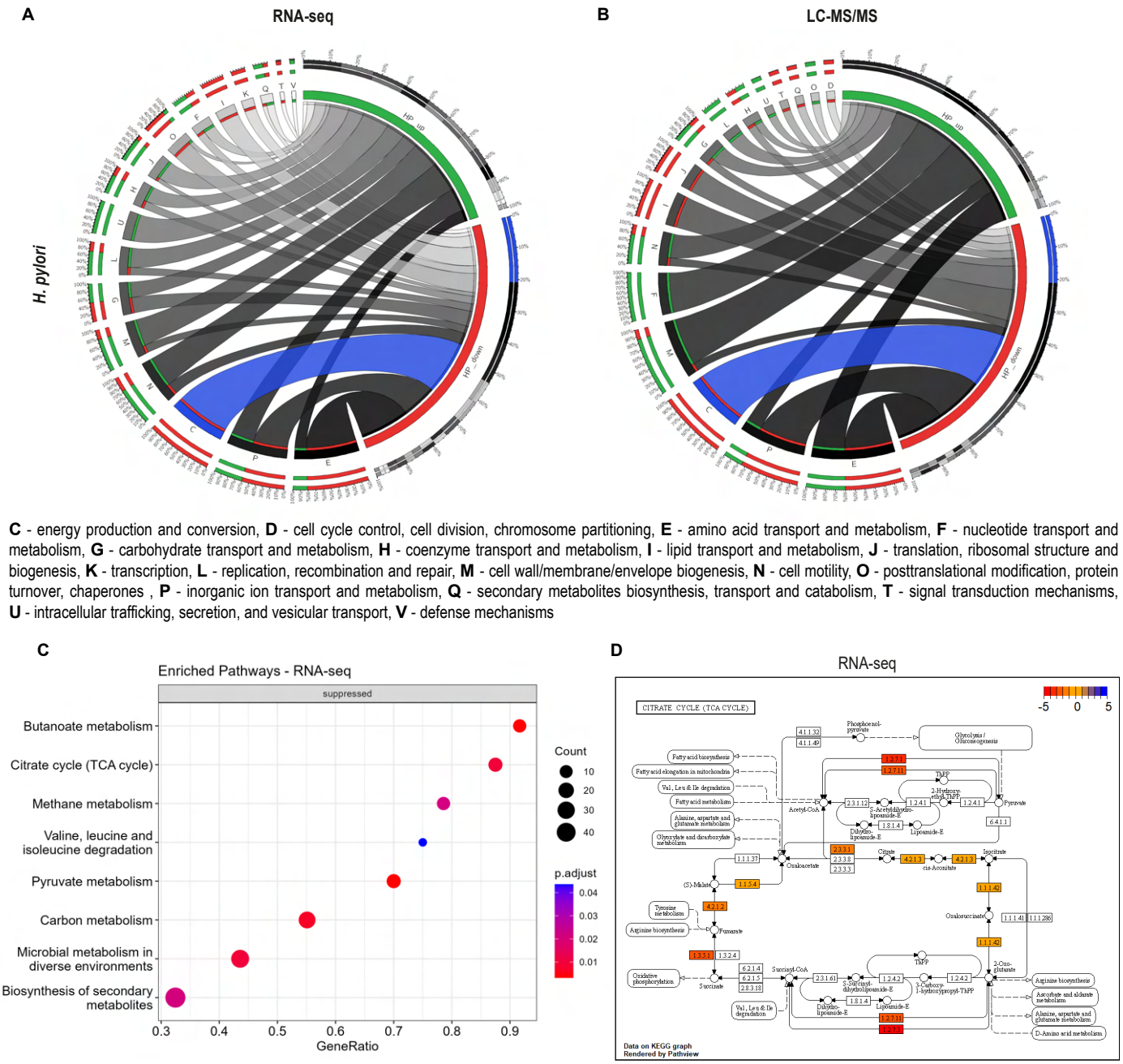

C - energy production and conversion, **D** - cell cycle control, cell division, chromosome partitioning, **E** - amino acid transport and metabolism, **F** - nucleotide transport and metabolism, **G** - carbohydrate transport and metabolism, **H** - coenzyme transport and metabolism, **I** - lipid transport and metabolism, **J** - translation, ribosomal structure and biogenesis, **K** - transcription, **L** - replication, recombination and repair, **M** - cell wall/membrane/envelope biogenesis, **N** - cell motility, **O** - posttranslational modification, protein turnover, chaperones , **P** - inorganic ion transport and metabolism, **Q** - secondary metabolites biosynthesis, transport and catabolism, **T** - signal transduction mechanisms, **U** - intracellular trafficking, secretion, and vesicular transport, **V** - defense mechanisms

S10 Fig. Impact of HP1021 on gene regulation in *H. pylori*. **(A)** Circos plots presenting the correlation between Cluster of Orthologues Group (COG) and differentially expressed *H. pylori* genes revealed by RNA-seq ($|\log_2 FC| \geq 1$ and FDR ≥ 0.05) in the *HP1021* knock-out mutant (ΔHP1021) strain compared to the *H. pylori* wild-type strain. **(B)** Circos plots presenting the correlation between COG and differentially expressed *H. pylori* proteins revealed by LC-MS/MS ($|\log_2 FC| \geq 1$ and FDR ≥ 0.05) in the ΔHP1021 strain compared to the *H. pylori* wild-type strain. **(C)** ClusterProfiler gene enrichment plot showing suppression of KEGG groups revealed by RNA-seq in the ΔHP1021 strain compared to the *H. pylori* wild-type strain. **(D)** Gene enrichment of citrate cycle KEGG group visualized by ClusterProfiler. Gene expression values are mapped to a gradient color scale of $\log_2 FC$. **(A-D)** Data prepared based on (7).

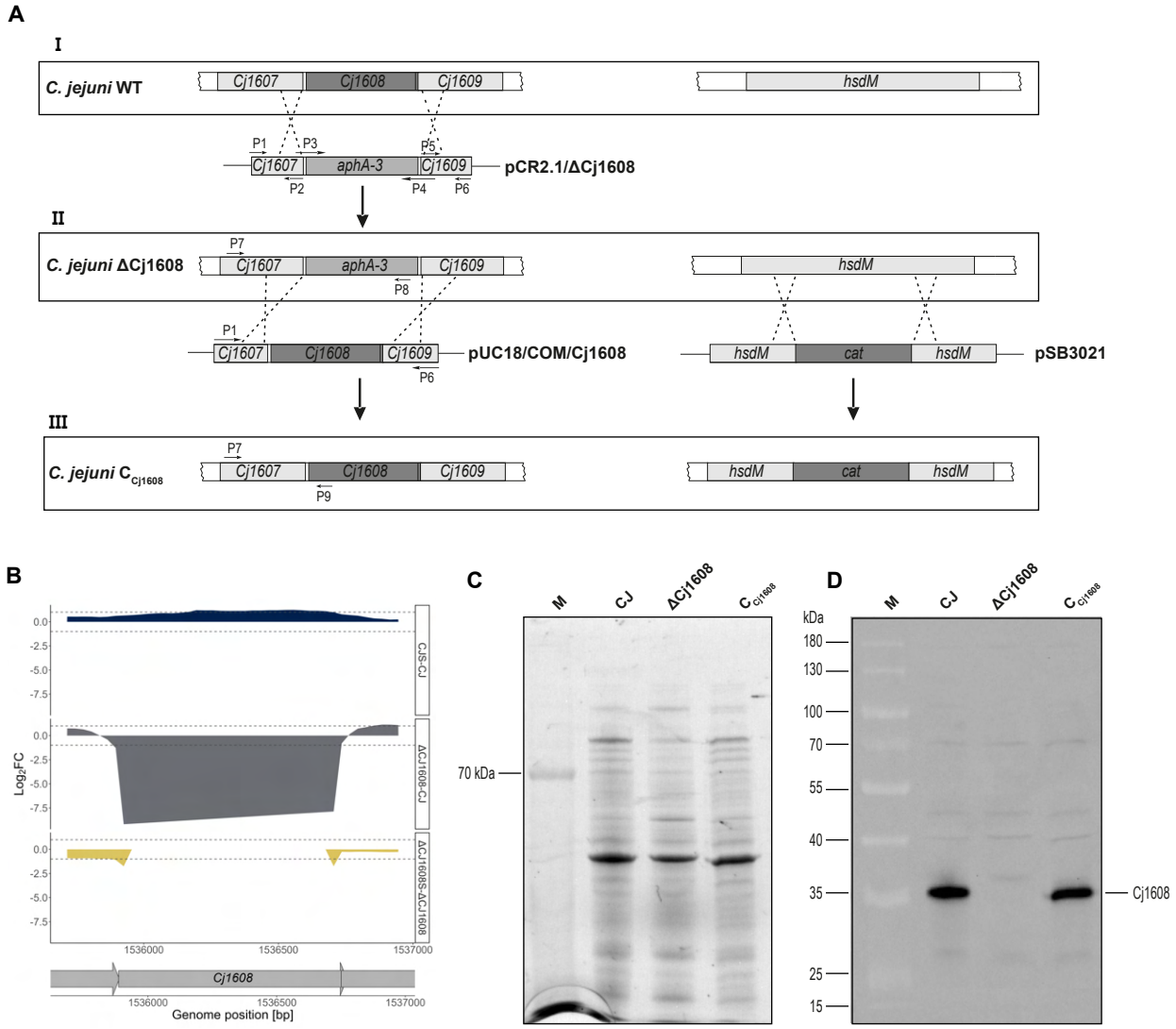

S11 Fig. *C. jejuni* NCTC 11168 ΔCj1608 knock-out mutant construction. (A) The mutagenesis strategy used to delete and subsequently complement Cj1608 on the *C. jejuni* chromosome. For the plasmids and primer sequences, see S1 Table and S2 Table, respectively. **(B)** RNA-seq data profile of Cj1608 gene of *C. jejuni* wild-type (CJ) and ΔCj1608 strains with the expression comparison. **(C)** Western blot analysis of Cj1608 in CJ and ΔCj1608 and complementation (C_{Cj1608}) strains. Lysate of each strain was resolved in a 10% SDS-PAGE gel and visualized by the TCE-UV method. **(D)** Cj1608 was detected in bacterial lysates by a rabbit polyclonal anti-StrepCj1608 antibody. M, PageRuler Prestained Protein Ladder (Thermo Fisher Scientific). Digital processing was applied equally across the entire image.

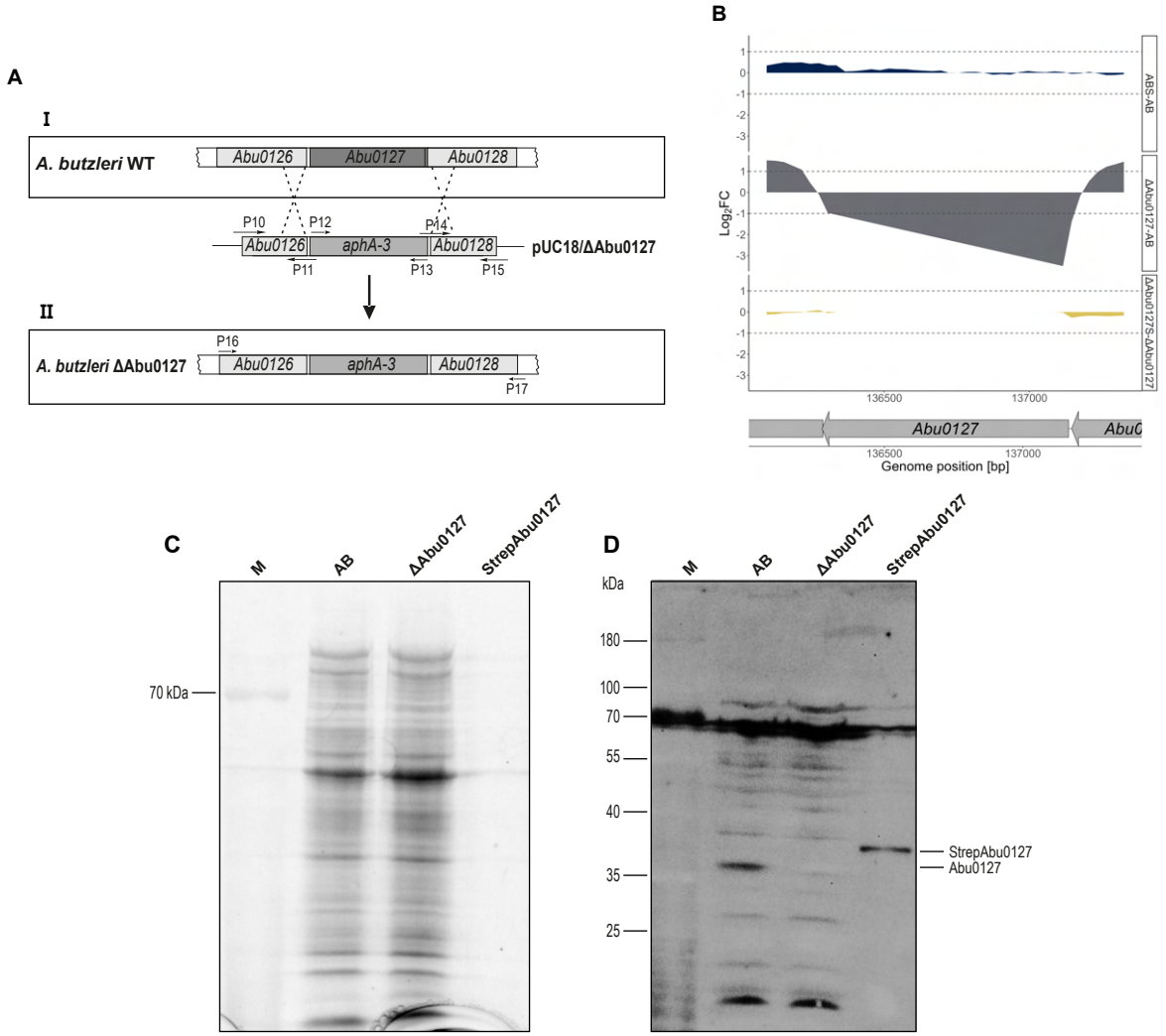

S12 Fig. *A. butzleri* RM4018 ΔAbu0127 knock-out mutant construction. (A) The mutagenesis strategy used to delete Abu0127 on the *A. butzleri* chromosome. For the plasmids and primer sequences, see S1 Table and S2 Table, respectively. **(B)** RNA-seq data profile of Abu0127 gene in *A. butzleri* wild-type (AB) and ΔAbu0127 strains with the expression comparison. **(C)** Western blot analysis of Abu0127 in AB and ΔAbu0127 strains. Lysate of each strain was resolved in a 12% SDS-PAGE gel and visualized by the TCE-UV method. 2.5 ng of StrepAbu0127 was used as a positive control. **(D)** Abu0127 and StrepAbu0127 were detected by a rabbit polyclonal anti-StrepAbu0127 antibody. M, PageRuler Prestained Protein Ladder (Thermo Fisher Scientific). Digital processing was applied equally across the entire image.

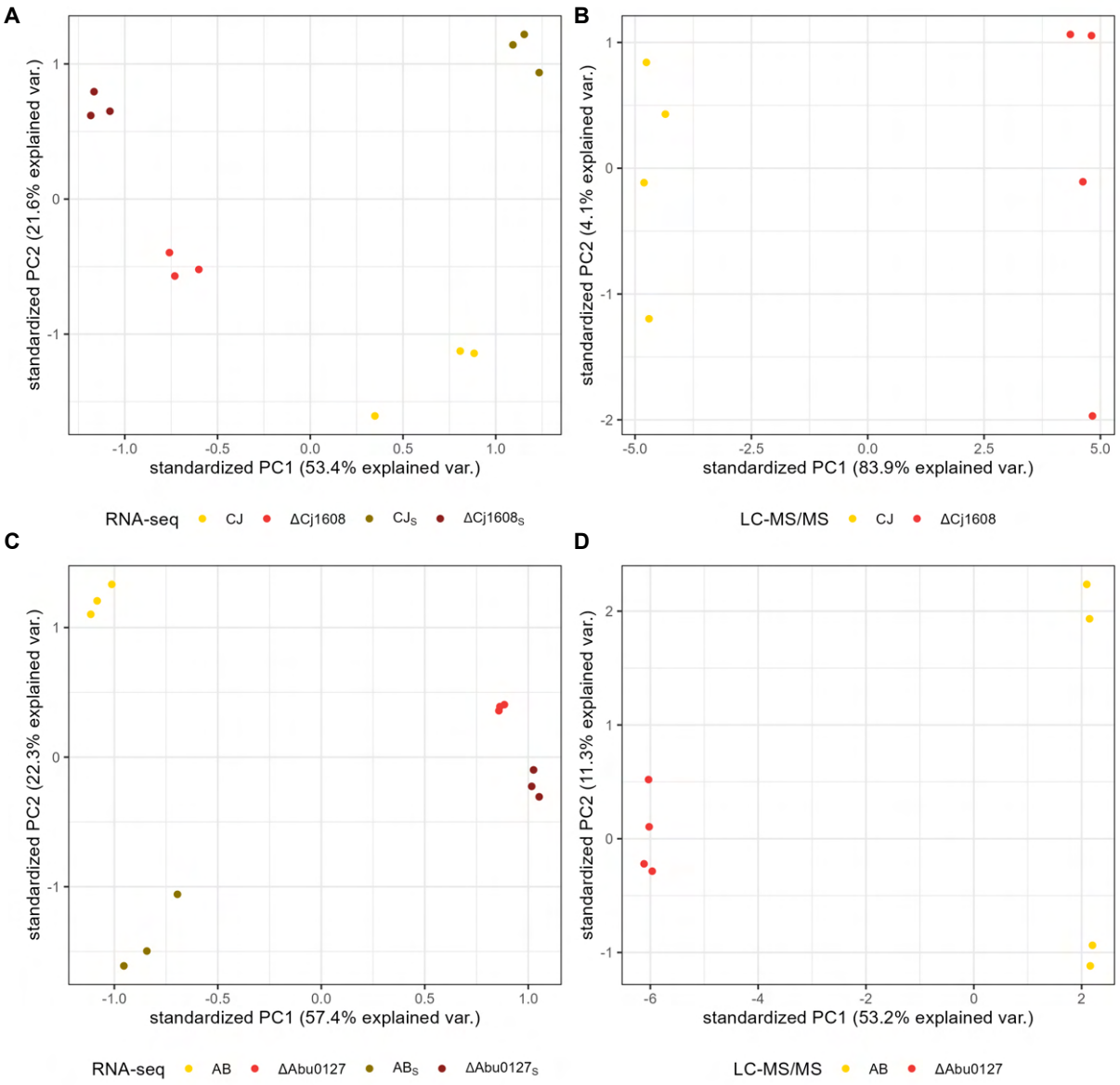

S13 Fig. The reproducibility of *C. jejuni* and *A. butzleri* biological replicates in omics data. (A) Principal component analysis (PCA) of the normalized RNA-seq CPM data of *C. jejuni* wild-type (CJ) and Cj1608 knock-out mutant (ΔCj1608) strains under microaerobic and paraquat-induced oxidative stress conditions (CJ_S and $\Delta Cj1608_S$). **(B)** PCA of the normalized LC-MS/MS CPM data of CJ and ΔCj1608 strains under microaerobic conditions. **(C)** PCA of the normalized RNA-seq CPM data of *A. butzleri* wild-type (AB) and Abu0127 knock-out mutant (ΔAbu1027) strains under microaerobic and paraquat-induced oxidative stress conditions (AB_S and $\Delta Abu0127_S$). **(D)** PCA of the normalized proteomics CPM data of AB and ΔAbu1027 strains under microaerobic conditions.

Description of Additional Supplemental Materials

S1 Data. Analysis of Cj1608-dependent gene expression in *C. jejuni* WT and Cj1608 knock-out mutant (ΔCj1608) strains under microaerobic and oxidative stress conditions. RNA-seq and LC-MS/MS data are presented. Genes are annotated according to the *C. jejuni* NCTC 11168 strain (NC_002163.1).

S2 Data. Analysis of Abu0127-dependent gene expression in *A. butzleri* WT and Abu0127 knock-out mutant (ΔAbu0127) strains under microaerobic and oxidative stress conditions. RNA-seq and LC-MS/MS data are presented. Genes are annotated according to the *A. butzleri* RM4018 strain (NC_009850.1).

S3 Data. Comprehensive RNA-seq and LC-MS/MS data results for genes of selected processes or pathways in *C. jejuni* and *A. butzleri*. Part of the data was compared to *H. pylori* omics data from (7). Transcriptomic and proteomic data are presented as $\log_2$-fold changes. Legends specific to each pathway/process were added below particular tables.

The Additional Supplemental Materials are available in open access under the link https://journals.asm.org/doi/10.1128/msystems.00784-24 and on the CD (Appendix) attached to the dissertation.

Supplemental Material References

1. Sambrook J, Russel DW. 2001. Molecular Cloning: A Laboratory ManualCold Spring Harbor Laboratory Press. Cold Spring Harbor Laboratory Press, New York.
2. Parkhill J, Wren BW, Mungall K, Ketley JM, Churcher C, Basham D, Chillingworth T, Davies RM, Feltwell T, Holroyd S, Jagels K, Karlyshev A V., Moule S, Pallen MJ, Penn CW, Quail MA, Rajandream MA, Rutherford KM, Van Vliet AHM, Whitehead S, Barrell BG. 2000. The genome sequence of the food-borne pathogen Campylobacter jejuni reveals hypervariable sequences. Nature 2000 403:6770 403:665–668.
3. Miller WG, Parker CT, Rubenfield M, Mendz GL, Wösten MMSM, Ussery DW, Stolz JF, Binnewies TT, Hallin PF, Wang G, Malek JA, Rogosin A, Stanker LH, Mandrell RE. 2007. The Complete Genome Sequence and Analysis of the Epsilonproteobacterium Arcobacter butzleri. PLoS ONE 2.
4. Szczepanowski P, Noszka M, Zdot;yła-Uklejewicz D, Pikuła F, Nowaczyk-Cieszewska M, Krężel A, Stingl K, Zawilak-Pawlik A. 2021. HP1021 is a redox switch protein identified in Helicobacter pylori. Nucleic Acids Research 49:6863–6879.
5. Watson RO, Novik V, Hofreuter D, Lara-Tejero M, Galán JE. 2007. A MyD88-Deficient Mouse Model Reveals a Role for Nramp1 in Campylobacter jejuni Infection. Infection and Immunity 75:1994.
6. Cieślak M. 2021. Construction of the plasmid for the analysis of the essentiality of the Abu0127 gene for the survival of Arcobacter butzleri RM4018. Wroclaw University of Science and Technology .
7. Noszka M, Strzałka A, Muraszko J, Kolenda R, Meng C, Ludwig C, Stingl K, Zawilak-Pawlik A. 2023. Profiling of the Helicobacter pylori redox switch HP1021 regulon using a multi-omics approach. Nature Communications 2023 14:1 14:1–14.

2.2.1. Co-authors' declarations of publication II

10.07.2024

Declaration

I, Mateusz Noszka, hereby declare that my contribution to the following manuscript:

Noszka, M., Strzałka, A., Muraszko, J., Hofreuter, D., Abele, M., Ludwig, C., Stingl, K., Pawlik, A., *CemR atypical response regulator impacts energy conversion in Campylobacteria*. **mSystems** 0:e00784-24 (2024), doi.org/10.1128/msystems.00784-24,

is correctly characterized in the table below.

Contributor	Description of main tasks
Mateusz Noszka	**Conceptualization:** throughout project implementation. **Methodology:** implementation of RNA-seq and ChIP protocols for *Campylobacter jejuni* and *Arcobacter butzleri*, as well as a protocol for *A. butzleri* mutagenesis. **Investigation:** conduction the experiments presented in the work, except LC-MS/MS analysis of proteins, NGS (RNA-seq) sequencing (both analyses performed on biological material I prepared), and EMSA for *Campylobacter jejuni*. **Formal analysis and Software:** statistical data analysis except for LC-MS/MS and NGS; NGS code modifications under Agnieszka Strzałka supervision; ClusterProfiler, Pearson correlation and Circos code preparation. **Visualization**: preparation of all results for publication, including data collection, analysis (in cooperation with co-authors), and preparation of figures and tables - Fig. 1, 2, 4, 5, 6, S1, S2, S3, S4, S5, S6, S7, S8, S9, S10, S11, S12, S13, Tab. S1, S2, Supplementary Data 1 and 2. **Data curation:** Supplementary Data 1-2; RNA-seq data deposition in ArrayExpress and GitHub. **Supervision:** co-supervision of Eng student Kinga Surmacz and MSc student Maria Cieślak. **Writing:** preparing a manuscript draft, participating in proofreading the manuscript, and preparing responses to reviewers. **Funding acquisition:** subproject 0000466 of the EPIC-XS, Project Number 823839, funded by the Horizon 2020 Program of the European Union.
Agnieszka Strzałka	**Methodology, Formal analysis and Software:** bioinformatic analysis of the RNA-seq data. **Investigation and Visualization:** code preparation for most NGS and LC-MS/MS plots. **Validation:** NGS data. **Supervision:** PhD student Mateusz Noszka in bioinformatic analyses. **Writing:** manuscript review and editing.
Jakub Muraszko	**Investigation:** EMSA for *C. jejuni*; co-investigation of the ATP level, growth curves and ChIP analyses. **Writing:** manuscript review and editing.
Dirk Hofreuter	**Validation and Formal Analysis**: Theoretical knowledge support. **Writing:** manuscript review and editing.
Miriam Abele	**Methodology:** mass spectrometric experiments and bioinformatic analyses of the LC-MS/MS data. **Data curation:** LC-MS/MS data deposition in ProteomeXchange Consortium. **Validation:** LC-MS/MS data. **Writing:** manuscript review and editing.
Christina Ludwig	**Methodology:** bioinformatic analysis of the LC-MS/MS data. **Writing:** manuscript review and editing. **Funding acquisition:** EPIC-XS, Project Number 823839, funded by the Horizon 2020 Program of the European Union.

Kerstin Stingl	**Conceptualization, Methodology and Resources:** construction of the first *C. jejuni* ΔCj1608 mutant strain, support in *C. jejuni* work. **Validation and Formal Analysis**: Theoretical knowledge support. **Writing:** manuscript review and editing.
Anna Pawlik	**Conceptualization:** initial project proposal and throughout project implementation. **Visualization:** Fig. 3 and Supplementary Data 3. **Validation and Formal Analysis**: throughout project implementation. **Data curation:** Supplementary Data 3. **Supervision:** PhD student Mateusz Noszka, Eng student Kinga Surmacz and MSc student Maria Cieślak. **Validation:** throughout project implementation. **Writing**: preparing a manuscript draft, reviewing and editing, and preparing responses to reviewers. **Funding acquisition and Project administration:** OPUS 17, Project Number 2019/33/B/NZ6/01648, founded by the National Science Centre, Poland.

.....

(co-author signature)

10.07.2024

Declaration

I, Agnieszka Strzałka, hereby declare that my contribution to the following manuscript:

Noszka, M., Strzałka, A., Muraszko, J., Hofreuter, D., Abele, M., Ludwig, C., Stingl, K., Pawlik, A., *CemR atypical response regulator impacts energy conversion in Campylobacteria*. **mSystems** 0:e00784-24 (2024), doi.org/10.1128/msystems.00784-24,

is correctly characterized in the table below.

Contributor	Description of main tasks
Mateusz Noszka	**Conceptualization:** throughout project implementation. **Methodology:** implementation of RNA-seq and ChIP protocols for *Campylobacter jejuni* and *Arcobacter butzleri*, as well as a protocol for *A. butzleri* mutagenesis. **Investigation:** conduction the experiments presented in the work, except LC-MS/MS analysis of proteins, NGS (RNA-seq) sequencing (both analyses performed on biological material I prepared), and EMSA for *Campylobacter jejuni*. **Formal analysis and Software:** statistical data analysis except for LC-MS/MS and NGS; NGS code modifications under Agnieszka Strzałka supervision; ClusterProfiler, Pearson correlation and Circos code preparation. **Visualization**: preparation of all results for publication, including data collection, analysis (in cooperation with co-authors), and preparation of figures and tables - Fig. 1, 2, 4, 5, 6, S1, S2, S3, S4, S5, S6, S7, S8, S9, S10, S11, S12, S13, Tab. S1, S2, Supplementary Data 1 and 2. **Data curation:** Supplementary Data 1-2; RNA-seq data deposition in ArrayExpress and GitHub. **Supervision:** co-supervision of Eng student Kinga Surmacz and MSc student Maria Cieślak. **Writing:** preparing a manuscript draft, participating in proofreading the manuscript, and preparing responses to reviewers. **Funding acquisition:** subproject 0000466 of the EPIC-XS, Project Number 823839, funded by the Horizon 2020 Program of the European Union.
Agnieszka Strzałka	**Methodology, Formal analysis and Software:** bioinformatic analysis of the RNA-seq data. **Investigation and Visualization:** code preparation for most NGS and LC-MS/MS plots. **Validation:** NGS data. **Supervision:** PhD student Mateusz Noszka in bioinformatic analyses. **Writing:** manuscript review and editing.
Jakub Muraszko	**Investigation:** EMSA for *C. jejuni*; co-investigation of the ATP level, growth curves and ChIP analyses. **Writing:** manuscript review and editing.
Dirk Hofreuter	**Validation and Formal Analysis**: Theoretical knowledge support. **Writing:** manuscript review and editing.
Miriam Abele	**Methodology:** mass spectrometric experiments and bioinformatic analyses of the LC-MS/MS data. **Data curation:** LC-MS/MS data deposition in ProteomeXchange Consortium. **Validation:** LC-MS/MS data. **Writing:** manuscript review and editing.
Christina Ludwig	**Methodology:** bioinformatic analysis of the LC-MS/MS data. **Writing:** manuscript review and editing. **Funding acquisition:** EPIC-XS, Project Number

	823839, funded by the Horizon 2020 Program of the European Union.
Kerstin Stingl	**Conceptualization, Methodology and Resources:** construction of the first *C. jejuni* ΔCj1608 mutant strain, support in *C. jejuni* work. **Validation and Formal Analysis**: Theoretical knowledge support. **Writing:** manuscript review and editing.
Anna Pawlik	**Conceptualization:** initial project proposal and throughout project implementation. **Visualization:** Fig. 3 and Supplementary Data 3. **Validation and Formal Analysis**: throughout project implementation. **Data curation:** Supplementary Data 3. **Supervision:** PhD student Mateusz Noszka, Eng student Kinga Surmacz and MSc student Maria Cieślak. **Validation:** throughout project implementation. **Writing**: preparing a manuscript draft, reviewing and editing, and preparing responses to reviewers. **Funding acquisition and Project administration:** OPUS 17, Project Number 2019/33/B/NZ6/01648, founded by the National Science Centre, Poland.

A. Stratka

.....

(co-author signature)